MEASUREMENT OF ACTIVITY-DEPENDENT RESPONSE TO ELECTRICAL STIMULATION IN SMALL UNMYELINATED AXONS

A Dissertation
Presented to
The Academic Faculty

By

Riley Thomas Zeller-Townson

In Partial Fulfillment
Of the Requirements for the Degree
Doctor of Philosophy in Biomedical Engineering

Georgia Institute of Technology and Emory University

December 2018

MEASUREMENT OF ACTIVITY-DEPENDENT RESPONSE TO ELECTRICAL STIMULATION IN SMALL UNMYELINATED AXONS

Approved by:

Dr. Robert Butera, Advisor
Wallace H. Coulter Department of Biomedical Engineering and the School of Electrical and Computer Engineering
Georgia Institute of Technology and Emory University

Dr. Garrett Stanley
Wallace H. Coulter Department of Biomedical Engineering
Georgia Institute of Technology and Emory University

Dr. Christopher Rozell
School of Electrical and Computer Engineering
Georgia Institute of Technology

Dr. Morten Raastad
Department of Physiology
Emory University

Dr. Bilal Haider
Wallace H. Coulter Department of Biomedical Engineering
Georgia Institute of Technology and Emory University

Date Approved: August 16, 2018

ACKNOWLEDGEMENTS

It took a village, but I'll be brief. I am thankful to have had a thesis committee with such a wide range of expertise. Dr. Garrett Stanley and Dr. Christopher Rozell were both pivotal in guiding my thinking on neural computation, first in classes and later as scientists who helped me to identify the value and appropriate context for my research, even with the breadth that I initially attempted. The later additions of both Dr. Bilal Haider and Dr. Morten Raastad to the committee helped me to see myself as a scientist, as I had initially encountered them both as authors of key papers on axon physiology. Their benchtop view of the axon was vital in helping me to understand the novelty and implications of the datasets I had acquired.

I have also been lucky to have worked with several research advisors. Dr. Steve Potter accepted me into his laboratory as a first year graduate student, and advised me through the initial stretch of my PhD. Working for Steve granted me a stunning degree of freedom as a graduate student to pursue a wide range of topics, spanning cellular neuroscience, artificial neural networks, art-science collaborations and neuroethics. It was a life changing opportunity, for which I am deeply thankful. Later, Dr. Andreas Hierlemann accepted me into his laboratory as a collaborator, largely due to the encouragement and advice of Dr. Douglas Bakkum. Working in the Hierlemann lab enabled me to use next-generation electrophysiology equipment that offered a radical new clarity to the research project I had started with Steve. Finally, when Steve unfortunately needed to leave his position, Dr. Rob Butera accepted me into his lab as a 6th year graduate student. Rob has been invaluable in helping me to focusing my PhD research, as well as to engage with a wider body of literature. I am indebted to him for his compassion and pragmatism.

This work was funded by NSF EFRI-COPN grant 1238097, NIH NINDS grant R01NS079757, and the ASEE SMART service for scholarship program.

TABLE OF CONTENTS

LIST OF FIGURES

LIST OF ABBREVIATIONS

AIS Axon initial segment

AP Action potential

BOTM Bayes-optimal template matching

CMOS MEA Complementary metal-oxide-semiconductor microelectrode array

DBS Deep brain stimulation

eAP Extracellular action potential

MEA Microelectrode array

TSS Triggered spontaneous scan

UMS2000 UltraMegaSort2000

SUMMARY

One of the most fundamental aspects of neurophysiology is that neurons are electrically excitable- that is, provided the appropriate electrical or sensory stimulus, they will respond by firing an action potential. This is well understood in both theoretical [1] and practical terms [2] for a single application of an electrical pulse to an otherwise inactive neuron. However, responses to sequences of stimuli, such as those used by clinical neural stimulators, can quickly become extremely difficult to predict. The problem emerges as each responding action potential activates a set of activity-dependent mechanisms, which in turn may alter the excitability of the neuron and therefore the number of action potentials evoked by stimulation[3]. As these activity-dependent processes are usually unmeasured, differ between neurons, and vary in their sensitivity to activity as well as their impact on excitability, the problem of predicting response to sequences of electrical stimuli is difficult to constrain. Here, we show how high-density microelectrode arrays, a novel electrophysiology tool, can be used to measure intermittent response to electrical stimulation. We then use these tools to probe the impact of the stimulus location relative to the neuron on intermittent response, and investigate the role of the delay between stimulus and action potential initiation in measurements of response latency. Based on these studies, we argue that intermittent responsiveness to stimulation is a phenomena governed by spatially local dynamics, rather than cell-wide dynamics. We then discuss implications of this claim for clinical neural stimulation, as well as the interpretation of antidromic latency measurements as evidence of timing plasticity.

CHAPTER 1
INTRODUCTION

One of the most fundamental aspects of neurophysiology, structuring both our understanding of what the nervous system does, as well as our experimental approach in studying it, is that neurons are electrically excitable. This manifests physiologically when a neuron is excited by a chemical signal detected at its synapses, and responds by generating an action potential, a milliseconds-long pulse of electrical current through the neuron's cell membrane. Nearly all of biological motion as we know it relies on the ability of individual neurons to transmit these action potentials across the span the body at speeds of meters per second, and upon delivery translate the message back into the language of chemical signaling. Neurons perform this feat using long, thin cellular appendages called axons which are highly specialized for this task. Other components of the neuron such as dendrites and soma first translate chemical signals into small electrical currents, which if strong enough will excite the voltage sensitive ion channels of the axon initial segment (AIS). Once excited, voltage sensitive ion channels allow more electrical current to flow into the neuron, amplifying and repeating the original electrical signal within the cell. This process then repeats as voltage sensitive ion channels spread throughout the axon are in turn excited by local currents, and generate new currents to excite their neighbors. Once a region of the axon has broadcast this pulse, it then begins the process of readying itself to send the next one.

Electrical methods are commonly used to not only detect the membrane currents of action potentials but also induce them, providing ways to causally study the effects of individual action potentials [4] as well as to rectify pathological activity[5]. The same electrical excitability of the voltage-sensitive ion channels within the axon membrane which allows them to repeat action potentials generated by their neighbors also means they will generate

action potentials in response to brief pulses of electrical current applied through nearby stimulation electrodes. In particular, extracellular stimulation, when used appropriately, can induce action potentials within axons with microsecond level temporal precision [6] and maintain stimulation reliability for up to years when implanted clinically.

While the physical process of neural excitation with extracellular stimulation is well understood in both theoretical [1] and practical terms [2] for a single application of an electrical pulse to an otherwise inactive neuron, responses to sequences of stimuli, such as those used by clinical neural stimulators, can quickly become extremely difficult to predict [7, 8]. This has major consequences for neural stimulation, as the sheer density and complexity of the nervous system means that most neural responses to electrical stimulation aren't ever observed. While extensive work in mathematical modeling of neural response to stimulation (e.g. [9, 10, 11]) has enabled the development of new clinical neural stimulation techniques in spite of a lack of direct observations, the lack of direct measurement has prevented a clear understanding of how current clinical stimulation techniques work, how they fail, and how they can be improved.

The complexities of responses in a single neuron to repeated electrical stimulation emerges as each responding action potential activates a set of activity-dependent mechanisms, which in turn may alter the excitability of the neuron and therefore the number of action potentials evoked by stimulation[3]. As these activity-dependent processes are usually unmeasured, differ between neurons, and vary in their sensitivity to activity as well as their impact on excitability, the problem of predicting response to sequences of electrical stimuli is difficult to constrain. Measurements of excitability dynamics *in vitro* have shown temporal correlations at time scales of seconds to many hours, suggesting that these relatively simple experiments engage many different activity-dependent mechanisms simultaneously [7]. The situation is exacerbated by the fact that responses to electrical stimulation are often measured through indirect means, such as population activity [12, 13, 14]. These measurements may confound stimulation reliability with other features of

neural response, such as action potential waveform or conduction velocity, which are also modulated by activity-dependent processes.

This thesis describes development of electrophysiology methods tailed to the observation of intermittent responsiveness to electrical stimulation, and then demonstrates the utility of these methodological developments in identifying constraints on the for the study of intermittent neural response to electrical stimulation. For the remainder of this chapter, we briefly review relevant literature on the mechanisms of clinical neural stimulation to motivate the importance of this topic. Chapter 2 gives an overview of the study of activity-dependent excitability, leading to a discussion on two currently unresolved questions within the field, and concludes with a brief review of the current methods available for resolving those questions. Chapter 3 describes how high-density complementary metal-oxide semiconductor microelectrode arrays, a novel electrophysiology tool, can be used to measure intermittent response to electrical stimulation. There, we demonstrate how the current state-of-the-art methods for extracellular axonal action potential detection can be improved through the use of an action potential latency estimator, and describe implications for the study of intermittent response to stimulation. We then use these tools to probe the impact of the stimulus location relative to the neuron on intermittent response in chapter 4, and investigate the role of the delay between stimulus and action potential initiation in measurements of response latency in chapter 5. Based on these studies, we argue that intermittent responsiveness to stimulation is a phenomena governed by spatially local dynamics, rather than cell-wide dynamics. In chapter 6 we discuss implications of this claim for clinical neural stimulation, as well as the interpretation of antidromic latency measurements as evidence of timing plasticity, and conclude in chapter 7.

1.1 Clinical neural stimulation

Despite their efficacy, the mechanisms by which clinical electrical stimulation induces therapeutic effects are not clear, and are active areas of research [15], [16]. At a high level, The

initial impact of clinical stimulation is the activation of neurons or neural elements near the stimulation electrode. Most stimulation activates axons[17], though careful design of the stimulus waveform used can be used to alter the targets of electrical stimulation [9]. Stimulation of the axon induces both orthodromic propagation, in the direction of normal AP travel, as well as antidromic propagation, towards the soma. These induced action potentials then interact with the spontaneous activity of the stimulated neurons, through collisions and conduction block. This acts to disrupt spontaneous pathological activity, such as by desynchronizing pathological synchrony. DBS effects are believed to be mediated by 'overriding' soma-generated pathological activity of deep structures, such as globus pallidus or subcallosal cingulate cortex, with tonic axonal activation [18, 19].

1.1.1 Clinical effects of neural stimulation rely on intermittent response to stimulation

DBS of the subthalamic nucleus in a rat model of Parkinson's disease causes responses to stimulation in motor cortex. While these neurons can be reliably stimulated at 10 Hz, the frequency with optimal therapeutic benefit is 130 Hz, which activates cells with low reliability. This particular frequency is also the point at which the induced firing rate of these stimulated neurons is highest[20]. Likewise, recording of excitatory post synaptic currents in neurons of substantia nigra compacta showed that therapeutic stimulation frequencies applied to subthalamic nucleus caused intermittent post-synaptic response, while non-therapeutic stimulation produced reliable response [13].

While it is expected that naturally occurring orthodromic APs would be annihilated by collision with stim-evoked antidromic APs, if stim-evoked antidromic propagation frequently fails at the axon it is possible that orthodromic propagation could travel a significant distance before failing. This would have substantial impact on the understanding of the mechanisms of clinical stimulators, constraining the location of the 'information lesion' to the stimulation site, rather than the entire neuron.

1.1.2 Neural responses to stimulation are activity-dependent

Importantly, these intermittent responses seen during clinical stimulation do not occur at all frequencies. Rather than using sub-threshold stimulation amplitudes, these protocols stimulate at amplitudes which are super-threshold when used for individual pulses, but through the recruitment of activity-dependent processes cause stimulation threshold to fluctuate. This is observed during subthalamic nucleus DBS, where the rate of axonal failure to respond increases with stimulation frequency [20]. This stimulation-frequency dependent reliability has been suggested to be extension of the refractory period [14], or to possibly be the result of activity-induced changes in extracellular potassium [21].

One especially interesting consequence of this change in excitability is that by stimulating neurons at rates faster than they can respond, they are kept at a state of being near their stimulation threshold. This may amplify the the stochastic nature of neural response to electrical stimulation, which usually appears deterministic for stimulation which is significantly higher than threshold. Stochastic effects can be leveraged to induce distinct firing patterns similar neurons using a single stimulus, which can be used to prevent pathological neural synchrony.

CHAPTER 2

BACKGROUND

2.1 Activity-dependent excitability

Axon conduction velocity and reliability are altered by neural activity (for reviews see [3], [22]). Such adaptation can include activity-dependent stimulation thresholds discussed in the introduction, but also include propagation failures, which have been observed in leech [23] and in hippocampal neurons *in vitro* [24, 25], as well as activity dependent conduction velocity (ADCV). ADCV is frequently observed at multiple timescales within individual neurons [26, 7]. When examined at the scale of single inter-spike intervals, these activity-dependent processes are studied in terms of the recovery cycle [27, 28, 29, 30], while changes in response to many action potentials are studied as activity-dependent slowing (ADS) [31, 25, 32].

2.1.1 The recovery cycle

The recovery cycle starts with the well-known absolute and relative refractory periods, which are caused by sodium channel inactivation and high potassium conductance[33]. These may be followed by a short period of supernormal excitability lasting up to 1 second in some preparations [34], where stimulation threshold is actually lower than resting conditions. The supernormal phase of excitability has been observed in caudatofugal axons of cat [35], callosal axons of monkey [36], and rabbit [37], as well as CA1 afferents of hippocampus [12]. In all of these cases, supernormal excitability was then followed by a period of subnormal excitability which lasted for a much longer period of time, ranging from seconds to minutes in some cases.

While the recovery cycle describes how excitability is modulated by individual action

potentials, sequences of action potentials in turn modulate the shape of the recovery cycle. These history-dependent effects can include enhancement of both the supernormal and subnormal periods of the recovery cycle [34], but the most common outcome is an extension of the subnormal period.

2.1.2 Changes in stimulation threshold are mirrored by changes in conduction velocity

In a variety of preparations, ranging from earthworm [27], rat unmyelinated sensor nerve [38], caudatofugal axons of cat [35], and schaffer collaterals [25], increases in stimulation threshold have been reported to be correlated with increases in the latency of response to stimulation. In several cases[39, 28, 25], this change in response latency has been measured to be proportional to the length of the propagation path, providing evidence that it primarily reflects a change in conduction velocity.

In some cases, an additional delay between the end of the stimulus pulse, and the beginning of a propagating AP in the axon ("AP initiation delay") may also be significant contributor to the total antidromic latency. Biophysically, this reflects the period of time where the axonal membrane voltage and sodium conductance begin their positive feedback loop, but before any part of the axon reaches peak AP voltage. Modeling work predicts that AP initiation delay [40] is especially large and variable [41, 42] when stimulus pulse amplitude is near the threshold for initiating an AP, growing as much as several milliseconds compared to stimulation that is far above threshold.

Normally this region of high latency, high variance initiation might be considered an edge case with little probability of occurring in the brain. However, during periods of intermittent stimulation failure, if the stimulation threshold of the axon adapts over repeated applications of the same stimulus, decreasing after stimulation failures and increasing after successful stimulation [25], the axon will be naturally driven toward this high latency, high variance regime.

2.1.3 AP waveforms change along with conduction velocity and excitability

A classic study on axonal branch points in lobster [23] found a 10-15% decrease in the amplitude of the intracellular voltage waveform of axonal action potentials, during a 25-30% decrease in conduction velocity induced by stimulation at 50 Hz. This decrease in the amplitude of the membrane voltage waveform was paired with a decrease in the amplitude of the membrane current waveform. Action potential amplitude was found to decrease during both antidromic and orthodromic propagation in this experiment.

Within the extracellular axonal recording literature, actual claims that eAP amplitude decreases during elevated firing rates are somewhat indirect. In most cases, this is due to the fact that measurements are coming from compound action potentials [12], and the amplitude of a volley is influenced by a variety of factors, most notably the reliability of activation. However, in cases where single axonal fibers can be recorded extracellularly, changes in eAP amplitude can be distinguished from changes in reliability. The eAP amplitudes of cultured cortical axons grown in PDMS channels were observed to decrease whenever stimulation latency increased during periods of repeated pulsed stimulation (10-160 Hz, 3000-4000 trials) [43]. Waveform width also increased substantially. When waveform amplitudes were shown alongside estimated conduction velocity, the two appeared so closely matched that they were summed together as a single measurement of 'signal fidelity' for further analysis.

One explanation for this observation of a tight connection between eAP width, amplitude and conduction velocity of single axons recorded extracellularly is that the changes in eAP waveform are consequences of changes in velocity. If we assume that the membrane current of the intracellular action potential waveform does not distort as it travels near the extracellular electrode, then the membrane current over the length of the axon will have the same waveform as the membrane current over time as recorded at any particular point on the axon, but scaled by the conduction velocity. As such, if changes in conduction velocity are not associated with major changes in the intracellular current waveform as measured

at a single point on the axon, eAP waveform width is determined entirely by velocity. As this scales the intracellular current waveform, a slowing-induced widening will also act to spread the same current over a wider region of the axon, causing peak action potential amplitude to decrease as well.

While the assumption that the membrane current waveform does not change during slowing is unlikely to be exact, any changes in membrane current waveform would act on top of this effect, which is a necessary outcome of the physics of extracellular recording. Further, modeling of the axon membrane using the the Hodgkin Huxley cable equation suggests that during subnormal conduction, AP membrane voltage waveforms currents show very minor changes in waveform[29].

2.2 Mechanisms of activity-dependent excitability

While there are several activity-dependent ionic currents by which action potential activity may translate to a change in excitability, many of them act through changes to resting membrane potential. Resting membrane potential has multiple impacts on excitability. Hyperpolarization of resting membrane potential generally increases the amount of stimulation current required to reach threshold, decreasing excitability and conduction velocity, while depolarization has the opposite effect. At especially depolarized membrane potentials, however, voltage-gated sodium channels will begin to inactivate. This has the inverse effect of decreasing excitability and conduction velocity. Most commonly, neural activity induces changes in membrane potential through pumps which are activated to reset ion concentrations in the wake of repeated spiking, such as the Na-K pump, as well as the Na-only pump. Hyperpolarization activated currents, also participate in shaping this process, as do a host of calcium mediated currents and slowly activated potassium currents.

An alternative mechanism for influencing excitability is the manipulation of ion concentrations. The concentration of potassium in the periaxonal space *in vivo* may increase in response to elevated levels of activity[12, 21], with potential impacts on conduction. While

such periaxonal ion concentration changes often some constraining factor (such as glia) to allow potassium to build up appreciably, intracellular ion concentrations have no such requirement. For thin axons in grey matter have high surface-to-volume ratios, there are relatively few action potentials required to change intracellular ion concentrations, such as accumulation of sodium. A recent modeling study [32] suggested that intracellular sodium concentrations could increase within a thin (0.25 μm diameter) superficial C fiber branch by as much as 50% after a single spike, leading to changes in the sodium reversal potential accrued over repeated stimulation at rates as low as Hz. Importantly, the thicker C fiber trunk was less impacted. This suggests that for neurons with especially thin collaterals, action potentials may induce an imbalance of intracellular sodium, which may then be re-set through passive diffusion of sodium from small compartments where concentrations quickly increased, into larger compartments which where relatively spared.

2.2.1 Activity-dependent excitability shows cell-type specificity

As conduction velocity is a property of the excitability of stretches of axon, it is impacted by nearly all of the excitability processes operating on the cell. As such, changes in latency can act as an 'excitability signature' of sorts, with different axons showing remarkable degrees of cell-type specific changes in latency in response to repeated stimulation. Activity dependent conduction velocity changes have been used to classify nerves fibers by function in the absence of immunohistological markers [44]. The sensitivity of peripheral nerve slowing to cell type is so fine that it is possible to distinguish between different classes of C fibers using latency trajectories alone [31]. This sensitivity appears to come from the susceptibility of different C afferents to slowing, rather than the rate at which different C afferents recover from slowing [30].

Small unmyelinated axons, such as Schaffer collaterals, are distinguished in their supreme sensitivity to stimulation at low frequencies, showing slowing at stimulation rates as low at 0.5 Hz, which is within their physiological firing rate range. [25]. The sensitivity of disso-

ciated cortical neurons grown in culture to slowing has also been seen to vary. Maximum stimulation following frequency was correlated with resting firing rate [43], suggesting higher firing rates may induce some sort of training effect in the cell, enabling it to more rapidly recover from the energetic load placed by an action potential. Despite this, neuron mean conduction velocity was found to not be significantly correlated with resting firing rate in a similar study [45], though was correlated with burst frequency and the number of spikes in a burst. Beyond this relationship between firing rate and conduction velocity stability, some neurons in dissociated cortical cultures show an increase in excitability shortly after the onset of activity-dependent slowing[43]. The degree to which this effect is instrinsic to the stimulated neuron and to which it is caused by other factors, such as stimulation electrode selection, is unclear.

2.3 Open questions in activity-dependent excitability

2.3.1 How does stimulation location impact activity-dependent changes in excitability of small axons?

Stimulation sensitivity varies across different cellular compartments at rest, but how does that sensitivity change during periods of elevated activity? Soma and dendrites are less sensitive to extracellular stimulation [46], and while the axon initial segment is the most sensitive to stimulation, the axon proper is believed to be the most common site of stimulation[17]. At elevated levels of activity, however, this may change. The thin diameter, and consequently higher surface-to-volume ratio of the axon may mean it is more sensitive to some mechanisms activity-dependent excitability than the AIS and soma, such as activity-dependent changes in intracellular ion concentrations [32].

2.3.2 Is initiation delay activity-dependent?

Thermodynamic ion channel noise induces fluctuations in resting membrane voltage, and can impact the reliability of AP initiation in response to stimulation. With smaller ion

channel counts, stochastic effects become amplified. This is apparent near stimulation threshold, as response probability decreases. As initiation delay has been described as being dependent on stimulation voltage relative to stimulation threshold, it is possible that activity-dependent changes to stimulation threshold increase the magnitude and variability of initiation delay.

2.4 Axonal electrophysiology with high-density microelectrode arrays

Measurement of the response of small axons to repeated electrical stimulation presents a technical hurdle. Studies *in vitro* have shown that individual cells which have been chemically isolated from their neural network can show significant trial-to-trial variation in their responses to stimulation protocols which are similar to those used in clinical neural stimulation[7], meaning that their measurement cannot rely on trial averaging. To address the impact of stimulation electrode location on these dynamics requires methods to precisely control location relative to the stimulated neuron's morphology, and understanding how this impacts conduction in different propagation directions will require the simultaneous measurement of action potential conduction at multiple sites along the axon. Further, thousands of such trials are necessary to capture the range of dynamics that occur during clinical neural stimulation, so methods need to have minimal impact on neuron health.

Traditional approaches to axon electrophysiology cannot meet these demands. Voltage sensitive dyes [47, 48], while capable of providing the spatial and temporal resolution necessary for such measurements, cannot do so with both the signal strength necessary for single-trial measurement and the low impact on cell health necessary to record for thousands of trials. Other voltage imaging modalities present similar problems, and may also alter the electrical properties of the neuron under study. While intracellular methods, such as patch clamp are able to accurately record action potentials in single trials and often with high specificity for a particular fiber, have a limited ability to sample from more than one region of the cell, and may also damage the cell. Sucrose- or grease-gap methods [49,

50, 51] can approximate the intracellular voltage of small fibers, but are also limited to usually one recording location and usually record from many small fibers simultaneously.

Traditional extracellular electrophysiology methods avoid the issues of toxicity and influence of the functional properties of axons, and have better temporal resolution than most voltage imaging methods. They can at times even provide the signal strength necessary to record axonal action potentials without the use of trial averaging [52]. However, traditional extracellular recording methods lack the spatial resolution necessary to register data from different axonal sites. This is a necessary step for measuring action potential propagation, rather than the simpler task of measuring the relative delays of individual action potentials that might be coming from different propagation paths or even different neurons.

Here, we use high density complementary metal-oxide-silicon fabricated micro-electrode arrays (CMOS MEAs) to study the impact of stimulation location on AP initiation in small unmyelinated axons. CMOS MEAs are tools that combine the temporal resolution and low impact on cell health of extracellular electrodes with the spatial resolution and sampling of microscopy. These tools can be configured to record from neurons at the network, circuit, and subcellular levels [53, 54, 55]. Previous work has demonstrated that by combining the results of many trials, they can be used to measure the extracellular electric 'footprint of action potentials, as well as the extracellular waveforms of up to millimeters of axon, identifying substantial variation in the baseline conduction velocity along the length of axons of dissociated cortical neurons [56, 57, 58], and the contribution of the axon initial segment (AIS) to the extracellular spike [59]. CMOS MEAs have also been used in single-trial mode to measure ADS at select locations along axons ([43, 46], as well as and the dynamics of stimulation reliability [46]. Given their spatiotemporal resolution and limited impact on neuron health, CMOS MEAs uniquely provide the necessary tools to disentangle the impact of stimulation location on AP initiation in small unmyelinated axons.

CHAPTER 3

PLATFORM DEVELOPMENT

3.1 Introduction

Comparing the activity-dependence of excitability and conduction velocity of small axons requires both highly specialized electrophysiology equipment capable of acquiring data from multiple locations along the axon, as well as analysis techniques capable of using these datasets to resolve the underlying biological signals. While well-established electrophysiology tools such as glass-substrate microelectrode arrays (MEAs) provide a limited ability to measure axonal signals directly [60], they cannot rival the spatiotemporal resolution high-density complementary metal-oxide-semiconductor fabricated microelectrode arrays (CMOS MEAs) [61]. While CMOS MEAs provide an extremely powerful and flexible hardware platform for performing these experiments [54], their novelty and complexity mean that many analysis approaches used on more traditional MEA systems may underutilize the capabilities of CMOS MEAs. Simply put, these devices haven't existed long enough for their full potential to be clear. As many routine experiments [62, 46, 56] on CMOS MEAs produce measurements of action potentials that could previously only be estimated with mathematical models [63], the development of new protocols and analysis techniques for this electrophysiology platform promises to open up new possibilities for empirical electrophysiology research.

In this chapter we describe developments in experiment protocol and analysis techniques for electrophysiology experiments performed on CMOS MEAs. These advances are motivated by two experimental objectives which CMOS MEAs show promise to enable, but which have not yet been met.

3.1.1 Experimental objective: measurement of orthodromic and antidromic action potentials within the same neuron

The first of these objectives is the measurement of orthodromic and antidromic action potential propagation within the same neuron. Such measurements which will be invaluable in the interpretation of decades of experimental research that has measured antidromic propagation [64, 39, 65, 66] in lieu of the more physiologically important, but difficult-to-measure orthodromic propagation. Prior work on CMOS MEAs demonstrated the feasibility of these experiments [56, 46, 43], but more recently experimental concerns were raised which call into question their practicality [67].

Below are desired features for measurement of orthodromic and antidromic action potentials within the same neuron.

Detection of axonal action potentials. The study of any activity-dependent phenomena necessitates some measurement of neural activity. While measurement of the large (¿100 μVpp) eAPs originating from the axon initial segment [59] and soma are usually sufficient for this purpose, during stimulation-evoked antidromic propagation, action potentials may propagate throughout the axon but fail to invade the soma [64]. As such, we need to be able to detect action potentials occurring within the axon only.

eAP measurement from axonal recording cites with known morphological relationships. Measurement of conduction velocity requires measuring the time an action potential occurred in at least two locations along the axon. Further, these compartments must be along the same propagation path, rather than on two separate branches of the same axon.

Control over stimulation location Measurement of the activity-dependence of propagation requires a method to control, or at least perturb neuron firing rate for minutes at a time. Comparing measurements of velocity across different propagation directions further requires being able to induce spikes propagating in different directions.

3.1.2 Experimental objective: measurement of intermittent axonal response to electrical stimulation

The second experimental objective is the measurement of intermittent response to repeated electrical stimulation of the axon [13, 14]. This promises to provide unprecedented experimental clarity in the study of neural response to clinically important stimulation protocols [20, 16]. Questions as fundamental as 'do apparent intermittent responses to clinical neural stimulation emerge from failures of the axon to respond to stimulation, or failures of the action potential to invade the soma?' are still active areas of research [20, 11], with contradictory evidence emerging from studies observing axonal stimulation response failures through indirect measurements on *in vitro* experiments [14, 68] and modeling experiments driven by advanced neural imaging techniques [11]. Again, prior work on CMOS MEAs demonstrated that intermittent response to electrical stimulation can be measured using these devices [43, 46, 67]. However, current approaches using advanced spike detection methods [69] still place bounds on the duration of these experiments [67], due to the loss of eAP signal strength which is generally observed in response to such stimulation protocols [12] [43]. As the dynamics of intermittent responsiveness to repeated electrical stimulation have been seen to change at a range of timescales from minutes up days [7], such constraints may prevent characterization of the effects of chronic electrical stimulation. Below are desired features for measurement of intermittent response to electrical stimulation in the axon.

Single-trial measurements. Averaging over trials or axons is often used to distinguish the small extracellular action potentials (eAPs) produced by axons from noise. However, changes in the amplitude of such averages may signify a decrease in either the reliability of response to stimulation, or a decrease or in the amplitude of reliable responses to stimulation. Single-trial methods are a high priority.

Minutes to hours long recording stability. The time course of activity-dependent slowing is up to minutes, so the measurements outlined above need to be repeated at stimulation frequency for hours at a time.

CMOS MEAs [54] directly enable some of these requirements. The CMOS MEAs [56] used in the experiments described in later chapters provide 11011 recording electrodes with 17 μM spacing between electrodes, providing the spatial resolution and spatial range to map out the extracellular field of an action potential over an entire neuron [62]. A nearly arbitrary subset of the electrodes can be routed to the 126 available recording channels [61], such that the array can be used to for either network level measurement of neuron firing rates [53], or sub-cellular level measurement of axonal action potentials [56].

3.2 Culturing

In this section, we briefly describe the necessary preparatory protocols to perform electrophysiology experiments on CMOS MEAs. The material is presented for the sake of completeness, and does not reflect original work.

3.2.1 CMOS MEA preparation

CMOS MEA chips were packaged onto interface printed circuit boards with 35 mm polystyrene dishes to create a reserve of cell culture media. Electrical contacts between the CMOS MEA and the PCB were insulated from media with epoxy (Epo-Tek 3023M, John P. Kummer AG, Cham, Switzerland, Epo-Tek 353ND and Epo-Tek 353ND/T, Fisher Scientific Co LLC, Pittsburgh, PA, US). Recording electrodes were electroplated with platinum black to decrease impedance and electrode noise. Electrodes were visually inspected for even platinum deposition.

CMOS MEAs were sterilized by soaking in 70% ethanol for 30 minutes and left to dry in a sterile laminar flow hood overnight. The CMOS MEA surface was prepared for cell adhesion by depositing polyethyleneimine (Sigma Aldrich Inc, St. Louis, MO, US) to im-

prove surface hydrophilicity, followed by the extracellular matrix protein laminin (Sigma).

3.2.2 Culture plating and maintenance

Rat cortical tissue from day 18 Sprague-Dawley embryos (Brainbits LLC, Springfield, Il, US) was dissociated enzymatically (Papain or Trypsin, both Sigma) and mechanically (trituration or vortex). For protocol details, see [70]. The resulting cell suspension was strained to remove large clumps of tissue, and then centrifuged in bovine serum albumin to remove cellular debris. Cells were counted and diluted in media to 1000-3000 cells/μL, with $\approx$20 μL of dilute cell suspension applied to each CMOS MEA. Cells were given 30-60 minutes of incubation time before flooding the reservoir with 2-3 ml of either plating media (Neurobasal) or culturing media (recipe from [71]). Cultures were maintained for several weeks in a sterile culturing incubator at 36.5 Celsius, 100$\%$ humidity, and 5$\%$ CO_2. Media was replaced once a week, or whenever pH changed noticeably due to culture metabolism.

Dissociated cortical cultures were used so that measurements of stimulus-evoked APs gathered here could be compared to the similar measurements made on lower-density glass-substrate MEAs [7]. Additionally, these cultures can be kept alive for as long as months, during which axonal signal strength tends to improve. Similar increases in axonal signal strength have been reported by plating neurons onto arrays pre-seeded with glia [60, 72], or by reducing the volume of media covering the culture and sealing the remaining media with mineral oil. This suggests that age-dependent increases in axonal signal strength are due to glial proliferation, electrically insulating axons from the culture media.

3.3 Electrophysiology

All recordings were done in an incubator at 36.5 Celsius and 5$\%$ CO_2. Relative humidity was kept at 60-70$\%$ to prevent damage to CMOS MEA electronics, and culture dishes were covered with gas-permeable lids made from polydimethylsiloxane. CMOS MEA temperature was kept stable, and within 0.3 Celsius of incubator temperature. Unless otherwise

noted, all experiments described here were performed in the presence of a mixture of synaptic blockers selected to prevent synaptically mediated correlations in activity between neurons (100 μM amino-5-phosphonopentanoic acid, 50 μM Bicuculline Methiodide, 10 μM 6-cyano-7-nitroquinoxaline-2, 3-dione, [56]). Cultures were given between 30-60 minutes to settle after being inserted into the incubator to allow time for the impacts of mechanical perturbation [73] and temperature transients to subside. Media was fully replaced after every recording experiment.

CMOS MEA channel configuration, data acquisition, and stimulation were controlled with the software suite MEAbench [74] and custom recording software written in MATLAB [75]. Electrode voltages were amplified 960x, bandpass filtered from 100-3.7 kHz, and sampled at 20 kHz with on-chip circuitry [56]. To minimize signal distortion and preserve signal strength, digital signal preprocessing prior to trial averaging was limited to DC offset correction (by subtracting the median recorded voltage), and stimulation artifact removal on stimulation electrodes using SALPA [76]. Electrode noise was measured to be between 10.11-28.9 μV_{RMS} prior to any digital filtering.

CMOS MEAs do not intrinsically provide better signal strength for axons, less recording noise, or more recording channels than many commercially available "low density" glass-substrate MEAs. Indeed, many of the techniques for recording axonal eAPs which were initially performed on CMOS MEAs have recently been replicated on MEAs with much lower electrode density[60]. However, as with tetrode arrays, the density of CMOS MEAs vastly improves our ability to distinguish action potentials originating from different neurons. Further, once eAPs in a particular region of the culture have been recorded at maximum electrode density, it is often possible to use only a few of those recording electrodes to sort action potentials with nearly the same accuracy [69]. This frees other recording channels to be allocated to electrodes at different locations, allowing for precise measurement of interactions between neurons [53].

An alternative application of this ability to precisely identify eAP sources while record-

ing from several locations at once, is the single-trial measurement of AP propagation along grown directly on the array[67]. Measuring AP propagation, by definition, requires detecting the same AP as it propagates to different sites along the axon. For extracellular recordings, which can detect signals originating from many different neurons, this also requires determining aspects of the identity of these signal sources. Signals must be verified to originate from the same neuron, and further from a contiguous axonal branch.

Once this is established, we also need to know what electrodes and voltages can be used to stimulate this shared axonal branch so as to induce propagation in different directions. The reconfigurability of CMOS MEAs allowed us to gather this data prior to each single-neuron experiment, through a sequence of preliminary experiments. This process, where one experiment informs the configuration of the CMOS MEA on the next, is diagrammed out in Figure 3.1. Note that the experiments described in this section are not novel in themselves, and references to the original papers describing them are provided. These experiments are described at length to provide appropriate context for the novel data analysis steps that follow.

3.3.1 Exp 1: Identification of spontaneously active neurons ("Spont Scan")

To find spontaneously active neurons on CMOS MEAs, spontaneous activity was recorded on all available recording electrodes (Figure 3.2a), using methods described in references [53] and [46]. All electrical recording and stimulation was performed relative to a large ground electrode submerged in media and outside of the array. As the CMOS MEAs we used [56] can only record from 126 out of their available 11011 electrodes on any given electrode configuration[61], recording from all available electrodes required a sequence of 95 recordings or 'scan.' By recording for 30-90 seconds on each configuration, the spontaneous firing rates and waveforms of large ($>50\mu$V, measured at the negative peak) extracellular action potentials could be gathered from up to 100s of neurons on the array. Spike detection and sorting was performed using UltraMegaSort2000 (UMS2000) [77, 78]

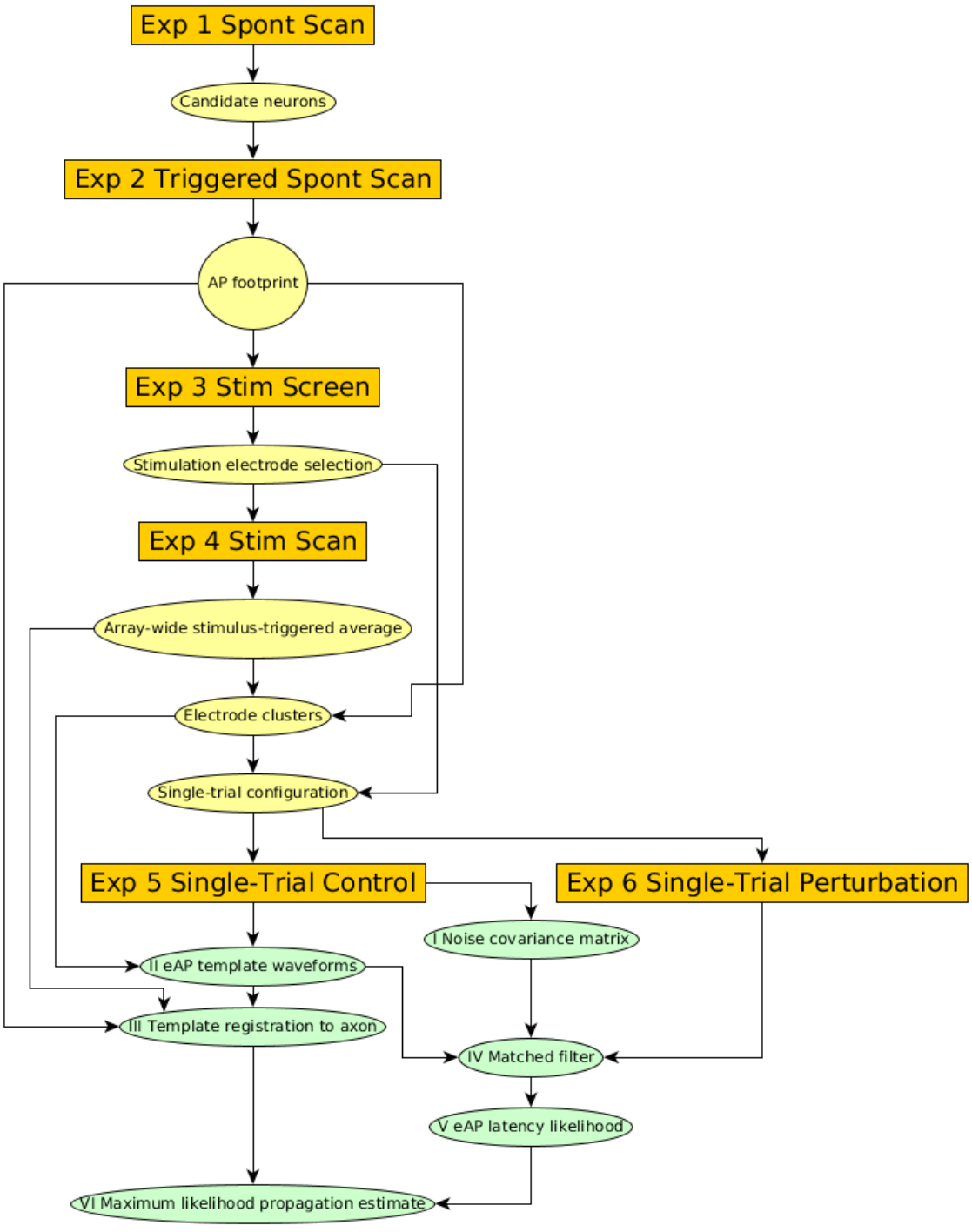

Figure 3.1: Flow chart for single-trial experiments. Individual experiments are identified with Arabic numbers and described in the 'Electrophysiology' section of the text. Computed inputs and outputs of each experiment are shown as yellow ellipses in the figure and are italicized when introduced in the text. Components of the latency estimator are identified with roman numerals, and are described in detail in section 3.4.

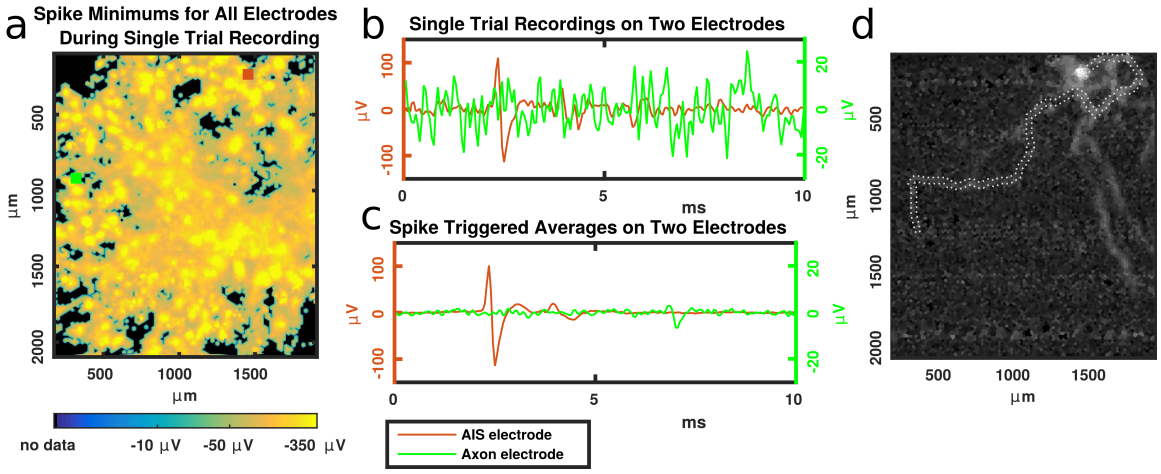

Figure 3.2: Finding axons using spontaneous activity. *(a)* minimum voltages recorded on all electrode on a CMOS MEA. *(b)* Single trial recording of a somatic action potential (red) and simultaneous recording at a second electrode (green). *(c)* Average of 60 somatic action potentials (red) and 60 simultaneous recordings (green) reveal a small axonal action potential on the second recording electrode. *(d)* minimum voltage of the spike triggered average on all electrodes creates a map of the axonal action potential, or AP 'footprint.'

using a threshold of 5x noise RMS. Once analyzed, these data provided a map of all the spontaneously active somatic action potentials which could be recorded from that culture, including information on amplitudes, optimal recording locations, and spontaneous firing rates.

Note that this experiment is routinely performed on developing cultures to monitor health and verify the success of the cell plating and CMOS MEA packaging steps preceding it. Such routine checks can be run for as little as 30 seconds per configuration, which means that neurons that rarely fire action potentials will likely be passed over, and estimates of spontaneous firing rate will be inaccurate. This lack of accuracy is acceptable when the goal is to merely verify that the culture has living, spontaneously active neurons, and to provide a rough estimate as to the density of recordable neurons on the array. In addition to this routine application, Spont Scans may also be used as the first step in a sequence of experiments aimed at finding axonal signals. In this case, the Spont Scan was usually run for 60-90 seconds per configuration to provide a more accurate estimation of firing rates.

3.3.2 Exp 2: Mapping axonal signals from individual neurons ("Triggered Spont Scan")

Once spontaneously active neurons were identified using a Spont scan, a subset of 15-30 were selected as *candidate neurons* for single-trial experiments. The first step of evaluating candidate neurons for single-trial experiments was to estimate each of their axonal eAP waveforms. This was done by calculating their somatic spike-triggered averages on all array electrodes, also called *AP footprints* [46], through the process described below. The resulting AP footprint is a template of an individual neuron's eAP waveform, as measured from all 11011 electrodes on the array. Importantly, this technique provides the primary data used to inform all subsequent electrode selection for stimulation and single-trial experiments.

Waveform estimation is usually performed by averaging many detected eAPs together to increase their signal to noise ratio (SNR), but axonal eAP amplitudes are too low to detect with conventional methods. While matched filters can be used to detect axonal eAPs [67], this paradoxically requires having prior knowledge of the shape of their waveforms. To create the AP footprint, axonal eAPs are instead 'detected' by detecting their associated somatic eAPs. Unless AP propagation fails, every occurrence of a somatic eAP will be followed by occurrences of all the axonal eAPs associated with that neuron. As such, a somatic spike-triggered average of a raw electrode recording will contain a blurred, trial average of any axonal eAPs which can be measured there. The degree of this blurring will depend on the precision of the propagation delay between the somatic and axonal eAPs, which has a jitter (standard deviation) of microseconds during spontaneous, non-bursting AP activity [67]. As such, it is unnecessary to correct this blur through peak-alignment techniques for the applications considered here.

Spontaneously active neurons identified exp 1 were selected based on their AIS AP amplitudes and firing rates (Figure 3.2, A). Neurons with larger AIS APs ($>200\mu$V) tended to be more responsive to electrical stimulation than those with smaller APs, and neurons with higher spontaneous firing rates (>5 Hz), tended to more reliably produce enough APs

during the triggered spontaneous scan to resolve their axonal APs.

AP footprints were created by measuring spontaneous activity using a specialized recording scan ("Triggered Spontaneous Scan", or TSS). As the goal is to create an array-wide spike-triggered average, each recording in this scan needed to be able to detect the somatic eAPs of all the candidate neurons, while also recording from as much of the remaining array electrodes as possible. To do this, we manually selected a set of electrodes sufficient to reliably detect the somatic APs for all candidate neurons, usually 1-3 electrodes per neuron (In red, Figure 3.2a). These electrodes were included in all the configurations used in the Triggered Spontaneous Scan, while the remaining unallocated recording channels were allocated to a different set of recording electrodes for each configuration. As these 'fixed' somatic recording electrodes took up 20-60 of the available recording channels, the TSS required as many as 400 configurations to scan most of the remaining array electrodes. Usually there were 100 or more electrodes out of the total 11011 available which could not be routed to recording channels at all during this process, due to the routing constraints placed by the somatic recording electrodes.

Once a set of array configurations was created, spontaneous activity was recorded for 60-90 seconds in each configuration, depending on the firing rate of the candidate neurons. Once the recording was completed, spike detection was performed on the set of fixed somatic recording electrodes as previously described. When found to be necessary from visual inspection of the detected waveforms, UMS2000's spike sorting tool was used to distinguish different action potentials recorded on the same electrodes.

Sorted spikes were then used to generate spike triggered averages for each electrode on the array (Figure 3.2b, c). Axonal APs could be measured after averaging 10-60 trials. If more than 60 action potentials were recorded in a given configuration, the 60 with the lowest instantaneous firing rates were selected, to mitigate the effect of activity-dependent conduction velocity variation on the trial average. All AP footprint recordings were done in the presence of synaptic blockers, to decorrelate AP firing times and prevent large fluc-

tuations in firing rate due to population bursts.

The resulting AP footprints (Figure 3.2d) include the extracellular APs for the axon initial segment, axon, and brief stretches of dendrites close to the soma [56, 46]. Axonal AP waveforms were identified by their shape (biphasic or triphasic with a relatively large negative peak in the center), small amplitudes (10-50 μVpp) and widths ($\approx$1 ms). Further, the propagation paths of these putative axonal AP waveforms showed stable amplitudes up to millimeters, corresponding to estimates of axonal AP amplitudes in dissociated cortical cultures [56].

Once AP footprints were calculated for each candidate neuron, a single *target neuron* was selected for subsequent stimulation experiments. Target neurons were selected by evaluating both the firing rate and somatic AP amplitude used for initial candidate neuron selection, along with the extent of the axonal arbor which could be visualized with the AP footprint. Footprints showing long (> 400 μm) stretches of axon which traveled away from the AIS were necessary, so that AP initiation at the axon and axon initial segment could be clearly distinguished. Additionally, reliable levels of spontaneous activity, $> \frac{1}{2}$ Hz, was desirable as this enabled monitoring of the neuron's spike triggered average over the course of the experiment. Often times a neuron with desirable footprint features was found to be unresponsive to electrical stimulation, in which case the candidate footprints were reevaluated to select a new target neuron.

There are other techniques besides the calculation of the AP footprint which can be used to identify axonal signals on CMOS MEAs. In particular, measurement of response to repeated, low-frequency (1-4 Hz) stimulation on randomly selected electrodes will often reveal a few axonal responses, which can be resolved by trial averaging. Once a single axonal waveform is identified in response to electrical stimulation, stimulation can be repeated with other recording electrodes to identify the spatial extent of the signal. This technique has been used on both CMOS MEAs [46] as well as traditional glass-substrate MEAs [60], and has the advantage of not requiring the axonal signal to originate from a

spontaneously active. While it does have the drawback that any responding axonal signals may have originated from any number of stimulated neurons, a much larger concern is that it requires a method to reliably identify axonal action potential signals in the presence of noise, without having a template of what waveform to expect. While such "anomaly detection" problems are the core of traditional spike detection, the combination of low signal strength and stimulation artifact make the task difficult to automate in practice. Manual monitoring of such responses can work quite well in healthy, active cultures [46]. However, when responses to stimulation are rare, either due to poor culture health or any number of other reasons, this technique becomes time consuming, and responses that do occur can easily be missed due to experimenter error. We instead used the TSS method described here as it could easily be run without manual intervention, and had the added benefit of providing a template of axonal signals originating from a single neuron when performed in the presence of synaptic blockers.

3.3.3 Exp 3: Stimulation electrode and voltage selection ("Stim Screen")

All stimulation was performed using pulsed, voltage-controlled, positive-first, biphasic square waves [2]. Biphasic voltage-controlled square waves were used as they are charge balanced, constrain voltage such that electrolysis can be prevented, and evoke temporally precise responses in neurons during their voltage downswing, rather than during one of their phases as is the case for current-controlled stimulation[79].

Stimulation electrodes were selected with the requirement that they showed a regional minimum for stimulation voltage threshold and could clearly be associated with either the axon or axon initial segment of the target neuron. Response to stimulation was detected either by measuring at electrodes near the axon initial segment of the target neuron using UMS 2000's spike detection tool, or by measuring axonal action potentials at other locations along the target neuron's axonal arbor using the tools described in the latency estimation section below. Peak sensitivity to electrical stimulation did not necessarily cor-

respond to the peak of the extracellular action potential, but stimulation sensitivity was generally higher near the peak of the recorded action potential [46] for both the AIS and the axon.

Stimulation threshold was estimated through an iterative procedure. On each iteration of the selection process, a stimulation amplitude was selected, and 10 stimuli of the chosen amplitude to each electrode separately, with an inter-stimulus-interval of 1 s. All stimulation was performed using positive-first biphasic square waves with phases each 200 μs long. Responses to stimulation on the target neuron were counted up, and all stimulation electrodes that evoked 10/10 responses advanced to the next round with a lower stimulation amplitude. This continued until the minimum stimulation voltage for the lowest-threshold electrode was identified. In some cases, the minimum stimulation voltage did not evoke a response at 100% reliability during subsequent 1 Hz stimulation. This was possibly a result of activity-dependent threshold adaptation at 1 Hz stimulation, or possibly due to the relatively wide posterior probability of reliability after measuring 10 successful responses. In these cases, stimulation voltage was then increased until a new minimum voltage was found, but the stimulation electrode was not changed. Note that generally, the minimum stimulation voltage was found to be lower for AIS stimulation than for axonal stimulation. Stimulation pulse peak-to-peak amplitude was kept less than 1 volt to prevent electrolysis.

3.3.4 Exp 4: Stimulation scan

After selecting a stimulation electrode and stimulation pulse amplitude which reliably evoked a response in the target neuron, we checked for *off-target eAPs* responding to the stimulus during another modified scan recording. In this case, the stimulation electrode was kept in all configurations, and the remaining channels allocated to different electrodes on each configuration in order to scan the array. Stimuli were applied 30-60 times for each configuration, with 1 second between each stimulus pulse to prevent activity-dependent changes to excitability. Synaptic blockers were used so that only directly evoked responses

to stimulation [2] would appear in the stimulation-triggered average.

The stimulation scan was then used to calculate an *array-wide stimulus-triggered average* (e.g., Figure 3.3). This showed the response of the target neuron to stimulation, as well as any off-target responses. On target response was distinct from the AP footprint of the target neuron when stimulation was applied near the axon, evoking antidromic propagation. Through detailed comparison of the AP footprint and stimulus-triggered average, we were able to identify electrodes where the target neuron's axonal eAP could be distinguished from off-target responses, even in cases where they had significant overlap. This was critical for studying axonal stimulation, where the stimulation voltages required to evoke reliable responses made activation of off-target neurons unavoidable for practical purposes.

3.3.5 Exp 5: Single-Trial Control

Once the impact of electrical stimulation was mapped out, we designed a single configuration to record responses of the target neuron to all further stimulation conditions. In order to detect axonal eAPs without trial averaging, single-trial configurations consisted of spatially separate *electrode clusters*, composed of densely packed electrodes[67]. Recordings from electrode clusters can be used to improve axonal eAP SNR by combining signal strength from nearby electrodes. Electrodes were selected for recording so as to maximize recorded signal strength of eAPs originating from a defined *axonal site* on the target neuron, minimize the number of off-target responses captured at that cluster (such as spontaneous or evoked action potentials from other neurons), and to maximize the length of the measurable propagation path (distance between clusters). Depending on the path of the target neuron's axon, a single electrode cluster could sometimes record from multiple axonal sites on the target neuron. These double-up clusters were used whenever the eAPs generated by these two axonal sites could be distinguished, improving the efficiency of the configuration.

After selecting clusters of recording electrodes and stimulation electrodes at the AIS

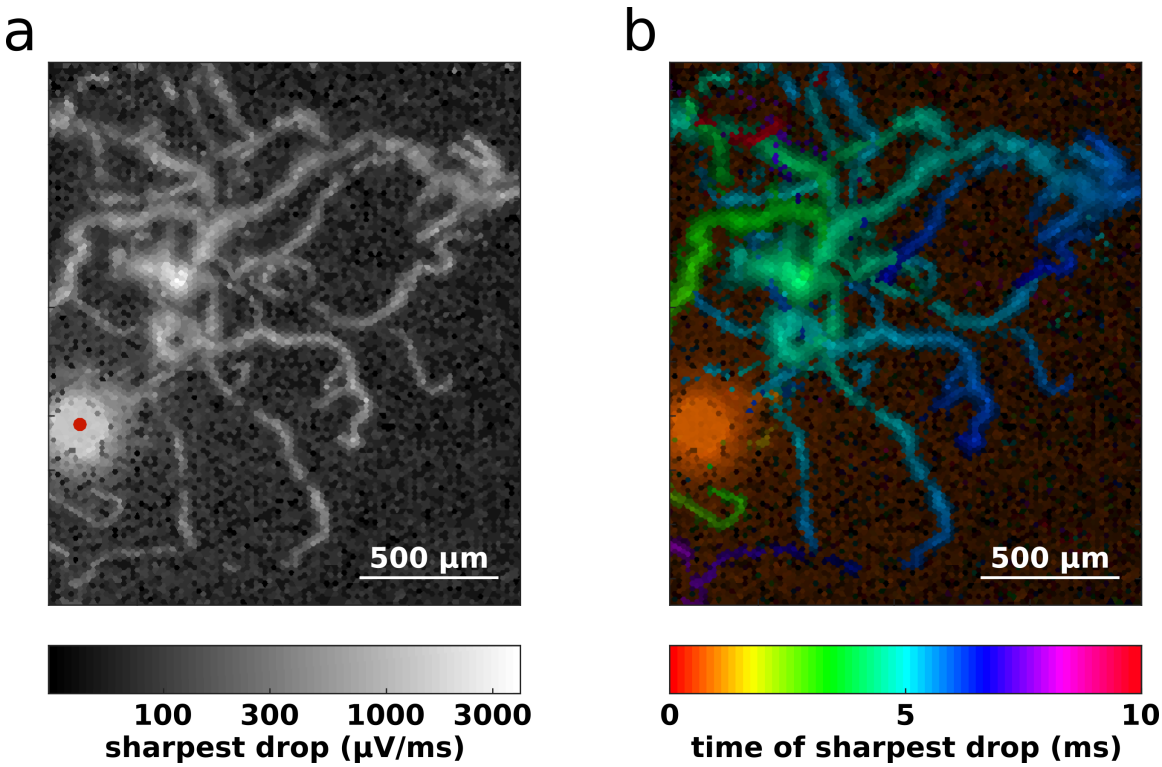

Figure 3.3: Stimulation-triggered array-wide scan. *(a)* greyscale image formed by finding the minimum of the temporal derivative for the stimulation-triggered average recording on each electrode. Stimulation electrode is marked in red. *(b)* false-color image showing the time at which the temporal derivative reached it's minimum. This shows the progression of AP propagation starting in a small axon below the stimulation electrode (in light green), propagating off the array, then back, before reaching the AIS and soma at 4.5 ms, and branching off in several directions.

and distal axon, stimulation was applied to the target neuron at each stimulation electrode for a period of 120 seconds at 1 Hz using the selected threshold voltage. 300 seconds of rest were included between each of these 120 second stimulation bouts. Stimulation at 1 Hz produced axonal eAPs with consistent stimulation latencies, which allowed them to be resolved by averaging over trials. These trial-averaged recordings were used to generate axonal *eAP templates* for subsequent filtering steps.

3.3.6 Exp 6: Single-Trial Perturbation

Once single-trial controls were complete, single-trial experiments measuring activity-dependent conduction velocity could begin. We drew our stimulation pulse frequencies from the activity-dependent slowing [3] and neuronal response latency literature [7], where slowing was observed at frequencies as low as 1-2 Hz, and intermittent failures to respond to stimulation were observed at frequencies as low as 5 Hz but occurred more frequently at higher frequencies. The highest stimulation frequency used in studies of intermittent stimulus response failures was 45 Hz [7], so we chose this frequency to study interactions between activity-dependent excitability and activation reliability dependent changes in neural activity. We used 2 minute long bouts of stimulation, at constant voltage and inter stimulus interval. 300 seconds of rest were included between each bout.

As with all axonal recordings on CMOS MEAs, axonal eAPs recorded during single-trial experiments could not be detected in raw data. However, unlike with the TSS and single-trial control recordings, analysis of these recordings cannot rely on the consistent timing relationships between axonal eAPs and stimulation or somatic eAPs which enable trial averaging. To estimate the latency of axonal APs recorded in these experiments, we used a combination of signal processing techniques described in the next section.

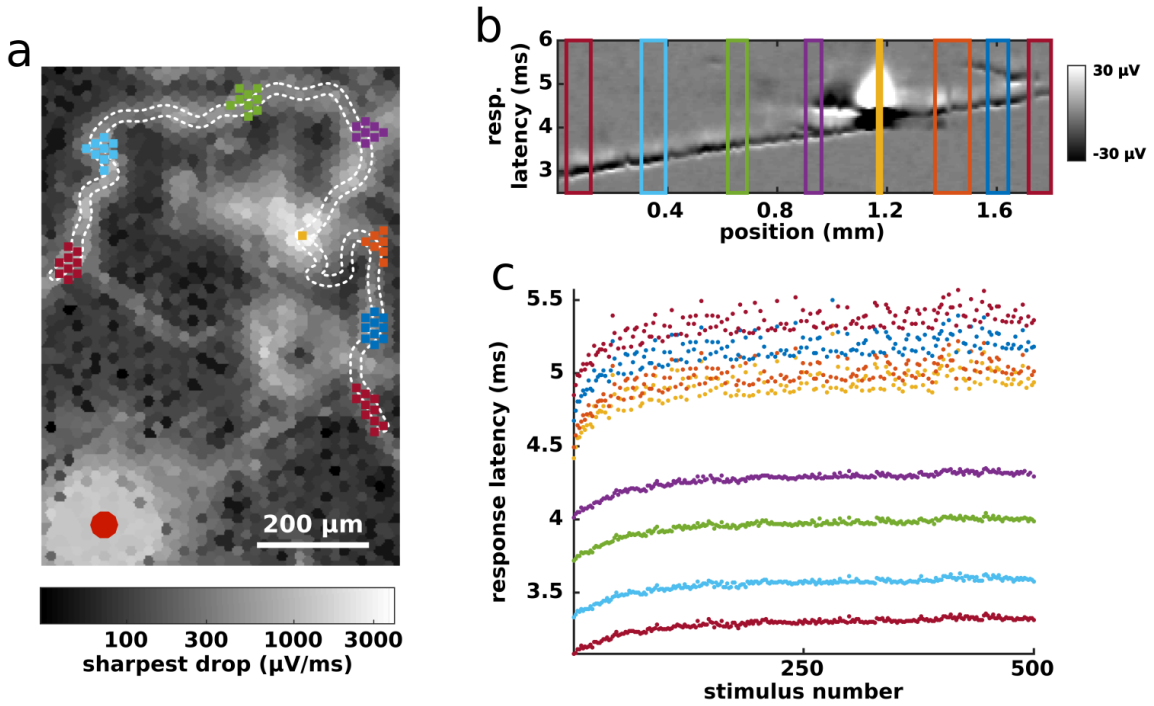

Figure 3.4: Recording stimulus-evoked action potentials along a defined propagation path. *a* close up on the stimulation scan image shown in figure 3.3*a*, showing the propagation path of an antidromic action potential evoked by axon stimulation. Electrode clusters used in a single-trial recording are shown as groups of colored squares along the putative propagation path, which is outlined with a white dashed line. *(b)* Stimulation triggered average for recording electrodes along the propagation path. Regions corresponding to electrode clusters are identified with rectangles of the appropriate color. Note the increasing latency of the axonal action potential as it travels from left to right along this path. The much larger extracellular action potential originating from the axon initial segment and soma saturates the image at the 1.2 mm mark. *(c)* Action potential latency estimates from stimuli applied at the stimulation electrode. Note the precision at which small trial-to-trial variations in latency are maintained in the first four recording clusters, which is lost once the AP reaches the AIS/soma starting at the fifth cluster (in yellow).

3.4 Latency estimation for propagating axonal APs

3.4.1 Why is detecting axonal action potentials on CMOS MEAs difficult?

Axonal SNR is near 1

The amplitude of the extracellular action potential (eAP) at the axon is quite small, with negative peaks ranging from 100 μV to less than 5 μV. As electrode noise is generally 11 μVrms, standard spike detection methods would prevent measurement of axons with amplitude less that 50 μV, the vast majority [67]. Further, methods capable of boosting the signal strength of axonal APs must also deal with the much larger signals (150-1000 μV) of the AIS/soma eAPs generated by nearby cells.

Antidromic activation prevents selective stimulation

While it is possible to find stimulation voltages which activate only a single neuron when stimulation is applied near that neuron's AIS [46], the higher stimulation thresholds at the axon make this selective activation practically impossible [67]. As such, when recording response to axonal stimulation, several axonal action potentials originating from different axons may be recorded on the same electrode cluster. These axonal action potentials must be sorted and and the target AP identified. In many cases several axons may bundle together to create 'micro fibers', with very similar propagation patterns in response to electrical stimulation. These similar propagation events must be distinguished through careful evaluation of the consistency of propagation in response to different stimulation locations, to ensure that all recorded eAPs originate from the targeted neuron.

Extracellular axonal AP waveforms are modulated during activity-dependent slowing

During activity-dependent slowing, extracellular AP waveforms recorded from axons tend to widen [43, 67]. From a signal processing perspective, this is a form of non-stationarity and implies that templates and thresholds calculated using data collected in one condition

may produce problematic results in other conditions. While this adaptation could be compensated for with an appropriate adaptive filter, this would be difficult to constrain without some prior understanding of the source of this adaptation and simplified ways to describe it. In lieu of this, methods that do not 'over commit' to one particular model of the axonal action potential are preferred.

3.4.2 State of the art: spike detection with matched filters

We started our analysis of axonal eAPs by using a Bayes-optimal template matching (BOTM) approach to spike detection, developed by Felix Franke, Milos Radivojevic and others for use with CMOS MEAs [69, 67]. This approach leverages the identified waveforms of APs recorded in electrode clusters through the use of a $matched\ filter$. As applied to spike detection, this technique creates a linear filter with the best possible separation between the spike and noise, using data originating from an arbitrary number of electrodes (Figure 3.5). Franke et al showed how this technique can be used to not only maximize spike detection accuracy, but also efficiently discriminate between (or sort) multiple action potentials recorded on the same set of electrodes [69]. They also showed how a Bayesian interpretation of the matched filter provides a clear method for optimal threshold setting. Radivojevic et al [67] then demonstrated how this technique can be used to record axonal action potentials along an axon with single-trial resolution, and by doing so identified sources of variability in axonal AP propagation. Here, we review their method, pointing out where we diverged from their approach, before discussing more extensive changes in the next section.

I. Noise covariance matrix

Working $in\ vitro$, we found that most signals measured on the CMOS MEA could be attributed to either eAPs or Gaussian noise, rather than non-eAP signals such as high-frequency oscillations. We did not observe stimulus-evoked high-frequency oscillations, as

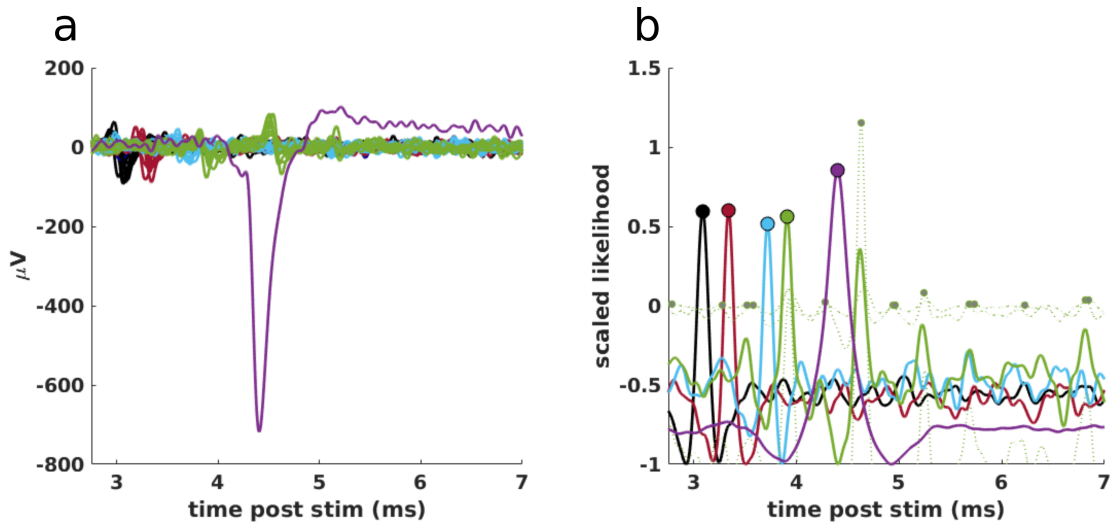

Figure 3.5: Bayes-optimal template matching for simultaneous spike detection and sorting. *(a)* Raw data recorded in response to axonal stimulation. Each electrode recording is color-coded by cluster. Note the much larger AIS eAP which is recorded on a single electrode, and which is preceded by a sequence of 4 eAPs on the other recording clusters at 3, 3.3, 3.7 and 3.9 ms. Also note that the recording cluster in orange shows more than one axonal eAP, including one 'off-target' eAP at 4.6 ms which is larger (approximately 160 μVpp) than the 'on-target' eAP at 3.9 ms (approximately 120 μVpp). *(b)* Matched filter outputs for the data shown in *a*. Filter outputs were scaled by cluster to aid in comparison, the original likelihood ratios were several orders of magnitude larger for the AIS cluster. Matched filters were created for each eAP which reliably occurred on each electrode cluster during 1 Hz stimulation, which included both on-target eAPs along the propagation path, as well as off-target eAPs. Filter outputs for eAPs along the propagation path are shown as solid lines, filter outputs for off-target eAPs are shown as dashed lines. For this set of recording clusters, only the cluster in orange showed multiple reliable action potentials. Local maxima which are above 0 are used as detected spikes. Note that the off-target eAP on the orange recording cluster causes the matched filter for the on-target eAP to cross threshold, but as the matched filter assigned to the off-target eAP produces a larger response the detected spike is identified as off-target.

have been reported on traditional glass-substrate MEAs [80]. Because of this, we elected to treat electrode noise as independent across recording electrodes, rather than calculate correlations between noise on different electrodes as performed by Franke et al [69] and Radivojevic et al [67]. This greatly reduced the dimension of the electrode covariance matrix which we needed to estimate from the data. Autocovariance was estimated using brief (3 ms, 60 samples) segments of data collected immediately prior to stimulation (120 trials).

II. eAP template waveforms

To create template waveforms to use in a matched filter, we manually identified AP waveforms from denoised multielectrode recordings.

Templates used for filtering a single configuration experiment were segmented from responses to control stimulation (1 Hz) applied using the same configuration. To resolve axonal APs, which usually have a signal-to-noise ratio (SNR) of near one, many recordings triggered by a single event (either a defined stimulation pulse, or AP detection on a particular electrode) were averaged together to boost SNR. Axonal APs could be measured after averaging 10-60 trials [56, 46]. All event-triggered AP footprints were calculated with data taken from experiments using synaptic blockers.

For each recording cluster, we collected template waveforms for all APs that reliably occurred in response to stimulation, including off-target APs. If multiple stimulation electrodes were used in an experiment, template sets were generated for each stimulation electrode. Data were then upsampled to 160 kHz, and aligned to compensate for sampling offsets between recording channels.

III. Template registration to axon

After all templates were segmented from the data, templates were manually registered against data recorded during stimulation scans to verify what part of the axonal arbor indi-

vidual templates corresponded to, and whether APs came from the target neuron or had resulted from the activation of an off-target neuron. This process was rather simple and could likely be automated for experiments with limited off-target activation of other neurons. For experiments where stimulation voltage was high enough to activate several cells, however, manual examination of putative propagation paths through sample-by-sample comparison of triggered spontaneous scans and different stimulation scans was required.

IV. Matched filter calculation

With slight deviation from the notation of [69], we define a recording window $L = 2r + 1$ samples, centered on sample t and recorded on electrode k as $\mathbf{x}(t)_k = [x(t-r)_k, x(t-r+1)_k, ..., x(t+r)_k]^T$. The template $\xi_{i,k}$ for eAP i recorded on electrode k can then be defined as the expected value of $\mathbf{x}(t)_k$ given eAP i occurred at sample t. We define eAP time using the negative peak of the eAP, or the sample with the maximum value for $\sum_k NRECT(\xi_{i,k})^2$, where $NRECT(x) = x$ if $x < 0$ and is equal to 0 otherwise, and the squaring operation is performed element-wise.

Unlike Franke et al, we calculate a unique covariance matrix C_k for each recording electrode k which is equal to $E[\mathbf{x}(t)_k^T \mathbf{x}(t)_k]$ for recording windows centered at t such that no eAPs are present in the window. As such, our filter can be calculated as $D_i(t) = \sum_k \mathbf{x}(t)_k C_k^{-1} \xi_{i,k} - \frac{1}{2}\xi_{i,k}^T C_k^{-1} \xi_{i,k}$. The noise covariance matrix was first regularized by discarding the principle components with the smallest 1% of the variance before being inverted.

3.4.3 Intrinsic problems with spike detection for latency estimation

Spikes detected and sorted using the BOTM approach provide a principled approach to the detection of eAPs originating from a specific source (the target eAP). However, traditional spike detection methods in general pose problems for estimating the latency of response to stimulation. The fundamental problem is that given a (potentially multi-electrode) record-

ing S samples long, a spike detector selects between 2^S possible outcomes. Every sample in the recording has two possible outcomes- that it either contains, or does not contain, an instance of the target eAP. Most of these possible outcomes, such as detecting 5 instances of the target eAP, are nonsensical in the context of estimating response latency. If we are tasked with estimating the latency of an eAP responding to stimulation, the target eAP can occur at most once, by definition. While it is possible that the neuron was spontaneously active, or that the stimulus induced a burst of activity within the target neuron, in these cases there is at most one instance of the target eAP and all other eAPs, even those occurring within the same neuron, are effectively background noise.

With a high enough signal strength, this mismatch between the behavior of the spike detector and the actual data we need for latency estimation is not a major concern. Each stimulus results in either an action potential or it does not, and deviations from this behavior due to either spontaneous activity or false positives can be detected by counting the number of detected eAPs between stimuli [43]. These problematic eAPs can then be removed on a trial-by-trial basis, or the occurrence of false positives on a subset of trials can be used to mark that particular recording location as unusable. However, for experiments where eAPs are small enough that even after filtering their signal-to-noise ratio (SNR) remains low ($>$25), false positives and false negatives may not be avoidable, and must be tolerated if the data is to be used. Indeed, in our experiments, only one dataset was collected where all measurements in response to control stimulation were free of false positives.

Further, even experiments where eAP SNR starts high enough to prevent detection errors (roughly 50+) may see substantial drops in signal strength and spike detection accuracy if they attempt to measure activity-dependent changes in conduction velocity and excitability. Such protocols tend to induce associated changes in eAP waveform width and amplitude. These deviations in eAP waveform from its shape at rest, and therefore from the shape of the template waveform in its associated matched filter, bias the detector toward false negatives. Errors in spike detection may also occur for a number of other reasons,

such as estimation errors in the covariance matrix or template, off-target action potentials which were not spontaneously active during the template-creation phase of the detection process, or drift in the waveforms of off-target eAPs towards the target eAP template. As such, methods which are robust to detection errors are needed.

3.4.4 Our extensions to state of the art: maximum likelihood latency estimation

To circumvent these issues, we took a maximum likelihood approach to estimate action potential latencies along the axon. We extend the BOTM method developed by Franke et al [69] and used by Radivojevic et al [67] by using their spike detector as the basis for a $latency\ estimator$ (section 3.4.4), which provides more flexibility for the analysis of stimulus-evoked responses we are focused on. The difference between these two classes of algorithm is in their outputs. Given a recording S samples long, a spike detector selects between two possible outcomes for each sample, corresponding to detecting a spike and not detecting a spike at that sample. For the entire recording, this constitutes a total of 2^S possible outcomes. With latency estimation, we add in the assumption that the spike of interest will happen at most once. This limits the number of possibilities considered, narrowing the problem down to selecting between $S+1$ possible outcomes- either the spike who's latency we wish to estimate occurred at any one of the S samples in the recording, or it did not occur at all.

In addition to providing estimates more suited to the analysis of stimulus-evoked eAPs, the latency estimator allows us to use the identified $propagation\ path$ the action potential takes as it travels from one recording location to another to improve estimation accuracy. Latency estimators, also called time delay estimators, have been developed for analysis of different electrophysiology techniques, including Electroencephalography [81, 82, 83], Electromyography [84, 85, 86, 87], Electrocardiography [88], and extracellular recording of peripheral nerve [89, 90, 91]. In most cases, these techniques leverage the fact that an unknown signal appears at two different locations at different times. For the latencies we wish

to estimate, this is not the case. Instead, we have a set of signals with well-characterized waveforms, and we merely wish to estimate their timing. The optimal approach in this case is to estimate waveform timing using the peak of the matched filter. We take an analogous approach by using the peak of the posterior distribution of eAP times, computed using the BOTM outputs.

Below, we describe how we adapted the BOTM spike detection approach to latency estimation. To do so, we first rearrange the detection and spike sorting performed through comparison of matched filter outputs in BOTM into a generalized likelihood ratio describing the likelihood of the latency of the target eAP. We then briefly describe how this shift in representation can be used to create a maximum likelihood estimate for the entire propagation path simultaneously.

V. eAP latency likelihood ratio

We can define this latency likelihood as $p(X|\theta_i)$, where X is a brief recording S samples long from an electrode cluster of K electrodes immediately following a stimulation pulse, and θ_i is the latency of eAP i in sample number. In practice, X corresponds to a recording lasting 5-22 milliseconds, so after upsampling S is between 800 and 3520 samples, and K is 1-40 electrodes. θ_i can take any integer value from 1 to S. All other possible outcomes of the trial, including off-target action potentials, form a second possibility, the null hypothesis that the action potential did not occur in the recording X. We will refer to this null hypothesis as the condition $\theta_i = \infty$, to distinguish it from the null hypothesis $\mathscr{M}_{0,t}$ considered by the matched filter. We then wish to calculate a likelihood ratio for latency estimation,

$$D_i^{lat}(t) = ln\frac{p(X|\theta_i = t)}{p(X|\theta_i = \infty)}$$

.

To do so, we used the matched filter output $D_i(t)$. $D_i(t)$ has the following statistical

interpretation:

$$D_i(t) = ln\frac{p(x(t)|\mathscr{M}_{i,t})}{p(x(t)|\mathscr{M}_{0,t})}$$

where $x(t)$ is the short window recording starting at time $t - j$, $\mathscr{M}_{i,t}$ is the hypothesis that this window was generated by the eAP template and some additive noise, and $\mathscr{M}_{0,t}$ is the hypothesis that this window was generated by noise alone. Note that $x(t)$ is the multielectrode version of $\mathbf{x}(t)_k$. In the case where there is only one eAP that may generate an action potential on a particular recording cluster, the matched filter output $D_i(t)$ is equal to $D_i^{lat}(t)$. This is as all data outside of the recording window surrounding time t will not be affected by whether $\theta_i = t$ or $\theta_i = \infty$, and inside the recording window $p(x(t)|\theta_i = t)$ is equal to $p(x(t)|\mathscr{M}_{i,t})$ to and $p(x(t)|\theta_i = \infty)$ is equal to $p(x(t)|\mathscr{M}_{0,t})$.

If however there are multiple action potentials which may occur on the electrode cluster, the matched filter will not suffice to calculate latency likelihoods, which is to say $D_i(t) \neq D_i^{lat}(t)$. On purely practical grounds, the matched filter will produce peaks when off-target eAPs occur. Statistically, the problem is that $p(x(t)|\theta_i = \infty)$ is no longer equal to $p(x(t)|\mathscr{M}_{0,t})$, as any of the other templates could have generated data within that window if $\theta_i = \infty$.

To resolve this, we need a model that describes the likelihood that any template besides the target template could have generated the data within the recording window.

$$D_i^{lat}(t) = ln\frac{p(x(t)|\mathscr{M}_{i,t})}{p(x(t)|\overline{\mathscr{M}_{i,t}})}$$

We do this by assuming a complete data model for the condition $\theta_i = \infty$. The goal here is to make this model flexible enough to include all possibilities that could be confused for the on target eAP i. Specifically, we allow for the $\theta_i = \infty$ condition to include the possibility that the recording window was generated by noise, or by any off target eAP m. Further, we include the possibility that any of the off target eAPs may occur within

some maximum offset Q from the center of the recording window. For a recording with M different off-target eAPs, this constitutes $M(2Q+1)+1$ hypotheses.

$$p(x(t)|\overline{\mathscr{M}_{i,t}}) = \frac{p(x(t), \overline{\mathscr{M}_{i,t}})}{p(\overline{\mathscr{M}_{i,t}})} \tag{3.1}$$

$$p(x(t)|\overline{\mathscr{M}_{i,t}}) = \frac{p(x(t), \overline{\mathscr{M}_{i,t}})}{p(\overline{\mathscr{M}_{i,t}})} \tag{3.2}$$

$$p(\overline{\mathscr{M}_{i,t}}) = p(\mathscr{M}_{0,t}) + \sum_{m} \sum_{j=-Q}^{Q} p(\mathscr{M}_{m,j}) \tag{3.3}$$

$$p(x(t), \overline{\mathscr{M}_{i,t}}) = p(x(t), \mathscr{M}_{0,t}) p(\mathscr{M}_{0,t}) \; + \sum_{m} \sum_{j=-Q}^{Q} p(x(t)|\mathscr{M}_{m,j}) p(\mathscr{M}_{m,j}) \tag{3.4}$$

To calculate the priors for this model, we can add the further assumption that each eAP template occurs on average once during the entire recording X. This assumption is reasonable for the case where templates correspond to reliably responding off-target eAPs. This sets the prior probability of each eAP occurring at any given sample to be $p(\mathscr{M}_{m,j}) = \frac{1}{S}$ for all values of m and j. The prior probability that a window is generated entirely by noise can then be set at $p(\mathscr{M}_{0,t}) = 1 - \frac{(M+1)(2Q+1)}{S}$

Calculating $p(x(t)|\overline{\mathscr{M}_{i,t}})$ requires knowing $p(x(t)|\mathscr{M}_{m,j})$ for all the off-target neurons, which we do not have direct access to. However, the output of the off-target matched filters $D_m(t)$ allows us to calculate a related quantity

$$\frac{p(x(t)|\overline{\mathscr{M}_{i,t}})}{p(x(t)|\mathscr{M}_{0,t})} = \frac{p(\mathscr{M}_{0,t}) + \sum_m \sum_{j=-Q}^{Q} exp(D_m(t)) p(\mathscr{M}_{m,j})}{p(x(t), \overline{\mathscr{M}_{i,t}})} \tag{3.5}$$

This is a version of the likelihood $p(x(t)|\overline{\mathscr{M}_{i,t}})$ which is scaled by the likelihood of the

noise $p(x(t)|\mathscr{M}_{0,t})$. We define the log of this scaled likelihood $D_\infty(t)$:

$$D_\infty(t) = ln\frac{p(x(t)|\overline{\mathscr{M}_{i,t}})}{p(x(t)|\mathscr{M}_{0,t})} \tag{3.6}$$

.

The outcome is that $D_\infty(t)$ is approximately equal to a 'softmax' operation performed on all the off-target eAP matched filter outputs. $D_\infty(t)$ can then be used to find $D_i^{lat}(t)$ using the matched filter $D_i(t)$ as

$$D_i^{lat}(t) = D_i(t) - D_\infty(t) \tag{3.7}$$

.

Once computed, the parameter t which produces a maximum value for $D_i^{lat}(t)$ can be used as an estimate of the true latency. If the maximum value of $D_i^{lat}(t)$ is less than 0, this implies that the maximum likelihood latency is $\theta = \infty$. Alternatively, as the number of possible latencies to evaluate is only as much as to the number of samples in the recording, it is possible to calculate the $D_i^{lat}(t)$ for every possible latency and use this information for further inference. In the next section, we show how the $D_i^{lat}(t)$ measurements at each axonal site can be combined to calculate the maximum likelihood latencies for all axonal sites simultaneously.

Note that a generalized likelihood ratio test could be used to resolve this problem. The difference there would amount to calculating $D_\infty(t)$ using the maximum likelihood hypothesis corresponding to $\theta_i = \infty$. While we initially experimented with the generalized likelihood ratio test, we found that the approach outlined here help to prevent overfitting of off-target eAP templates to the data, which had the negative consequence of obscuring low-amplitude eAP waveforms.

VI. Maximum likelihood propagation estimate

The latency log likelihood ratio $D_i^{lat}(t)$ described above was then used to calculate the likelihoods for valid conduction sequences, as shown in figure 3.6. We defined a valid conduction sequence as one where the eAP latency of each axonal site occurred in the correct order. For a sequence of C compartments with S post-stimulus samples, there are $(S+1)^C$ possible sets of spike latencies, which quickly become infeasible to enumerate. Frequently there are 10+ points in a conduction path, each with thousands of possible latencies after upsampling. Rather than evaluate every possible valid conduction sequence, an iterative process was used to identify a subset of possible sequences of spike latencies across different clusters on the array. Specifically, at each point in the conduction path, the maximum likelihood spike time (and associated likelihood) was calculated for all possible lower bounds on that spike time, and all possible upper bounds (a total of $\frac{1}{2}(S+1)^2$ evaluations, skipping cases where the upper bound is lower than the lower bound).

This set of spike times must contain the maximum likelihood spike time for that point in the conduction path, no matter what the other spike times are in the rest of the conduction path. Further, two such blocks of latency likelihoods from consecutive conduction path points can be combined into a third in an efficient manner, such that the maximum likelihood of latencies along the entire conduction path never requires comparing more than $(S+1)^2$ possibilities simultaneously.

3.4.5 Estimator outputs

The results of the analysis described above are a set of likelihoods, amplitudes, and latencies calculated for each recording compartment on each trial of the experiments. These measurements are the maximum likelihood latency estimate given the propagation hypotheses evaluated, the likelihood of the that compartment's data given that propagation hypothesis, and the amplitude of the action potential peak relative to control at the estimated latency. All subsequent data analysis was performed on these estimates.

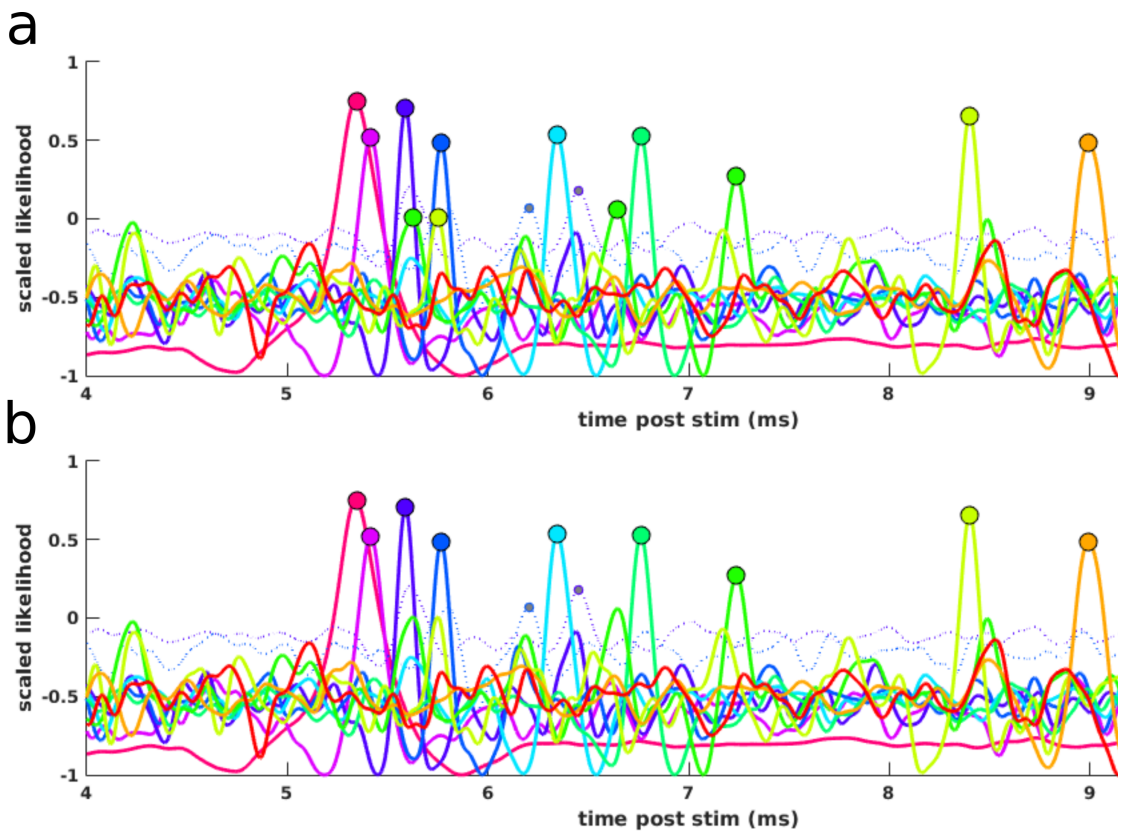

Figure 3.6: Impact of propagation sequence on spike detection. *(a)* Spike detection as described in Figure 3.5, using matched filter outputs for a sequence of 9 axonal eAPs at different electrode clusters. Note that due to their low signal strength, there are two false positives on the green cluster, and one false positive on the yellow. Also note however that the correct eAPs are detected on these clusters, and have stronger amplitudes than the false positives. *(b)* Maximum likelihood eAP latencies for propagation along this sequence.

3.5 Analysis of axonal AP latency estimates

The signal processing techniques used the previous section produce estimates of spike latency by finding the point in each trial that 'looks' most like the spike of interest, rather than noise or an off-target spike. Further analysis using this reduced-dimension description must contend with errors in this estimation process.

3.5.1 Consequences of AP latency errors

On trials where on-target AP propagation was not evoked, latencies from noise peaks approximate a uniform distribution when using the latency likelihood output, and a more complicated gamma-like distribution when using the maximum likelihood propagation time estimator. On trials where on-target AP propagation was evoked, noise spikes may still occur for individual compartments, if the AP amplitude of that compartment is low enough. In these cases, the noise peak latencies will be drawn from a uniform distribution with constraints set by maximum likelihood propagation estimator- namely the latencies of the APs of the previous and subsequent compartments in the propagation sequence. Because of this, the variance of these noise spikes will tend to be higher on the first compartment where a stimulation evoked AP is recorded, which tend to have a mean control latency of 1-2 ms after stimulation, compared to the mean latencies of 0.2-1 ms between compartments. Because spike times are not estimated independently on separate compartments, this increased variability of the latency at the first compartment does not necessarily translate to an associated increased variability at subsequent compartments.

Estimated amplitudes, which are derived from the estimated latencies, likewise follow different trajectories for these different sources. Importantly however, the amplitude of noise peaks follows a much more Gaussian-like distribution, which sets a lower bound on the lowest amplitude that can be measured from any other source. Because of this, noise peaks will always have a mean AP amplitude lower than the on-target AP, though

their mean latency will tend to be higher than on-target AP latency. The variance of the noise-peak AP amplitude will also tend to be much lower than the variance of noise-peak latencies.

Latencies of off-target APs produce more complicated effects than noise peaks. Their latencies follow the slowing profile of the off target compartment, which may be qualitatively similar to the on-target AP, though an offset can usually be seen. Importantly, changing off-target latencies may cause sudden shifts in the accuracy of the maximum likelihood propagation estimator, if the latency of a high-amplitude compartment enters into the latency constraint range of an adapted compartment. This may cause amplitude estimates to suddenly increase for a subset of propagation compartments, or potentially be in a state of switching back and forth between a high amplitude and low amplitude estimate for a set of trials.

3.5.2 Sources of AP latency errors

Analysis of AP latency estimates requires careful attention to sources of AP latency errors which might bias comparisons of derivative analytes.

Activity-dependent decreases in estimated AP amplitude increase the number of AP latency errors. At elevated stimulation frequencies, the amplitudes of all reliably evoked APs decreased, causing on-target and off-target responses to appear more like noise peaks, increasing the rate of misclassified APs. The notable exception to this rule was the spike detected at the axon initial segment during axonal stimulation, which though it's amplitude was observed to decrease during elevated stimulation rates was always clearly separable from the distribution of amplitudes corresponding to putative failures of the AIS.

Compartments in the distal axon are more prone to latency errors than compartments closer to the AIS. This is due to the tendency for extracellular action potential signal strength to decrease with distance from the axon initial segment.

For stimulation-evoked propagation in any direction, early recording compartments are

more prone to latency errors than later compartments. If stimulation is not selective to the target neuron, all off-target activation will emanate from the same stimulation location, and will consequently be expected to be densest at the earliest recording locations. The elevated number of reliably activated off-target APs increases the number of possible misclassifications. This early-compartment effect is a larger problem for axonal stimulation than AIS stimulation, as the axon often required higher stimulation voltages, increasing the number of off-target responses.

Error rate also depends on the effective search window for each eAP, as set by the eAPs preceeding and following it in the propoagation path. This potentially impacts the first recording compartment more than others due to the period immediately after stimulation where stimulation artifact prevents all spike detection (1-2 ms, compared to the usual delay of 0.2-1 ms between spike latencies on recording clusters). As a consequence, outliers at the first recorded compartment will tend to have a higher variance than those occurring at subsequent compartments. The last axonal sites in a propagation path also tend to have larger errors, as they have the fewest constraints on their maximum latencies.

Lastly, matched filters were only created for for action potentials which occurred reliably enough during the control condition that templates could be made. Errors could sometimes occur if elevated stimulation rates uncovered 'hidden' action potentials which were qualitatively similar to the on-target AP.

3.5.3 Stimulation reliability estimation

Stimulation reliability is of critical importance for all measurements of activity-dependent excitability, but can be surprisingly difficult to measure. If all latency estimates came from either on-target AP propagation or noise peaks, the best test statistic for separating stimulation failures and successes would be the maximum likelihood of any propagation event, less the likelihood of stimulation failure, as calculated by the maximum likelihood propagation estimator. For cases in which reliability estimation needed to be compared across different

stimulation locations, the test statistic was recalculated using only the AP compartments which could be recorded in both stimulation conditions. This prevented the much larger AIS AP (usually 150-1000 μV, compared to 5-100 μV for axonal APs) from biasing reliability estimates for axonal stimulation vs stimulation of the AIS, or for confusing failures of AIS invasion for axonal stimulation failures [65].

In most cases, inspection of estimated latencies quickly showed the presence of latency errors from off-target APs, which usually cause overestimates of reliability. To compensate for this, the test statistic was recalculated with the outlier-laden compartments removed.

Once a clean test statistic was created, the proportion of trials corresponding to stimulation failures, stimulation successes, or unclear needed to be estimated. If the tests statistic histogram clearly showed two non-overlapping distributions that could be verified to correspond to noise and on-target APs, this was done by manually setting a threshold and counting responses on either side. If the two distributions overlapped, the test statistic was fit to a Gaussian mixture model (number of components selected using the Bayesian information criterion), and mode proportions calculated. Modes were manually identified as corresponding to spikes, noise, or outliers, and reliability was estimated as the proportion of all spikes divided by the proportion of all spikes and failures. In some experiments a static Gaussian mixture model failed to distinguish spikes and noise due to the non-stationarity of spike amplitudes. To prevent underestimation of reliability in such cases, the test statistic was broken up into sets of 100 consecutive trials, which were each fit to separate 2 component GMM. Components were identified in a semi-supervised manner (using distance to previously identified components). In cases where a set of trials showed merged spike and failure distributions, the merged sets were excluded from further analysis.

3.5.4 Analysis of AP amplitudes

As extracellular AP amplitude has been observed to decrease during activity-dependent slowing and decreases in excitability[12, 43], measures of amplitude are useful as general

estimates of the degree of slowing which has occurred in a neuron. Further, amplitude has an advantage over latency in that errors in latency estimation produce more easily anticipated effects in amplitude error (analogous to clipping), and that the accuracy of amplitude estimates is not dependent on the length of axon being measured or the sampling frequency of the recording system.

Comparing amplitude under different conditions requires first selecting a compartment which can be measured under those conditions, and which also provides an unbiased comparison. Stimulation artifact usually prevents spikes from the first 1-3 axonal compartments in the propagation path from being detected, so shared compartments are always drawn from the central compartments of a propagation path. Even when a compartment could be recorded in multiple stimulation conditions there were many cases where the AP template signal strength, and thus the estimated AP amplitudes, differed across stimulation electrodes for the same compartment. This occurred due to differences in overlapping off-target APs in different conditions.

Comparing estimates of the minimum achieved amplitude are of special importance and difficulty. The minimum amplitude corresponds to the maximum degree of slowing, and if stimulation failures have also occurred in recording it provides insight into the magnitude of the activity-dependent effects which lead to stimulation failures, providing an estimate of the safety factor for stimulation. However, the trials with the minimum amplitudes are also the trials most likely to be misclassified as stimulation failures themselves. In many cases, no clear distinction could be made between heavily adapted spikes and noise, and so a proper minimum amplitude could not be calculated. In these cases, the most that can be gleaned from the data is that amplitude must have dropped at least as far as the mean noise-peak amplitude. The noise peak amplitude is itself set by the signal strength of the axonal compartment at rest and duration of the search window for that compartment. Note that because this lower limit is compartment-dependent, compartments with the same degree of slowing-induced amplitude decrease may appear to show very different amplitude

trajectories over time, if one compartment reaches it's measurement limit earlier.

3.5.5 Analysis of AP latencies

Similarly to amplitude, comparing changes in latency across stimulation conditions requires selecting compartments where latency can be recorded reliably under both conditions. However, in order to compare propagation delay across different stimulation locations, at least two shared compartments must selected. As with amplitudes, the compartments with the highest amplitude APs usually provide the most accurate estimates, though with latency measurement the distance between the selected compartments is also a contributing factor. Activity-dependent slowing generally does not cause propagation delays to increase by more than 50%, so the total change in latency measured during an experiment is proportional to the initial propagation time observed. As the sampling rate of the recording system and noise introduce some error into latency estimates, the 'signal to noise ratio' for slowing estimates is the square of the measured latency, divided by twice the recording error.

As latency errors due to noise peaks introduce much larger errors in latency than they do into amplitude, it was often necessary to restrict latency analysis to trials with a higher degree of certainty of occurrence. For latency analysis of antidromic data, only trials where the large spike at the axon initial segment was detected were used, as this spike constrains the search space for the smaller axonal spikes, which decreased the rate of misclassified action potentials. For orthodromic data, a variant of the test statistic used for reliability estimation was used, but using all available recording compartments. However, even with absolute certainty that the propagating AP had occurred, an action potential detected at a particular location along that path may have been incorrectly identified, introducing a large quantity of outliers. As such, for all analysis of AP latencies, we set amplitude thresholds for each axonal waveform. As shown in Figure 3.7, this greatly reduced the variance of recorded latencies.

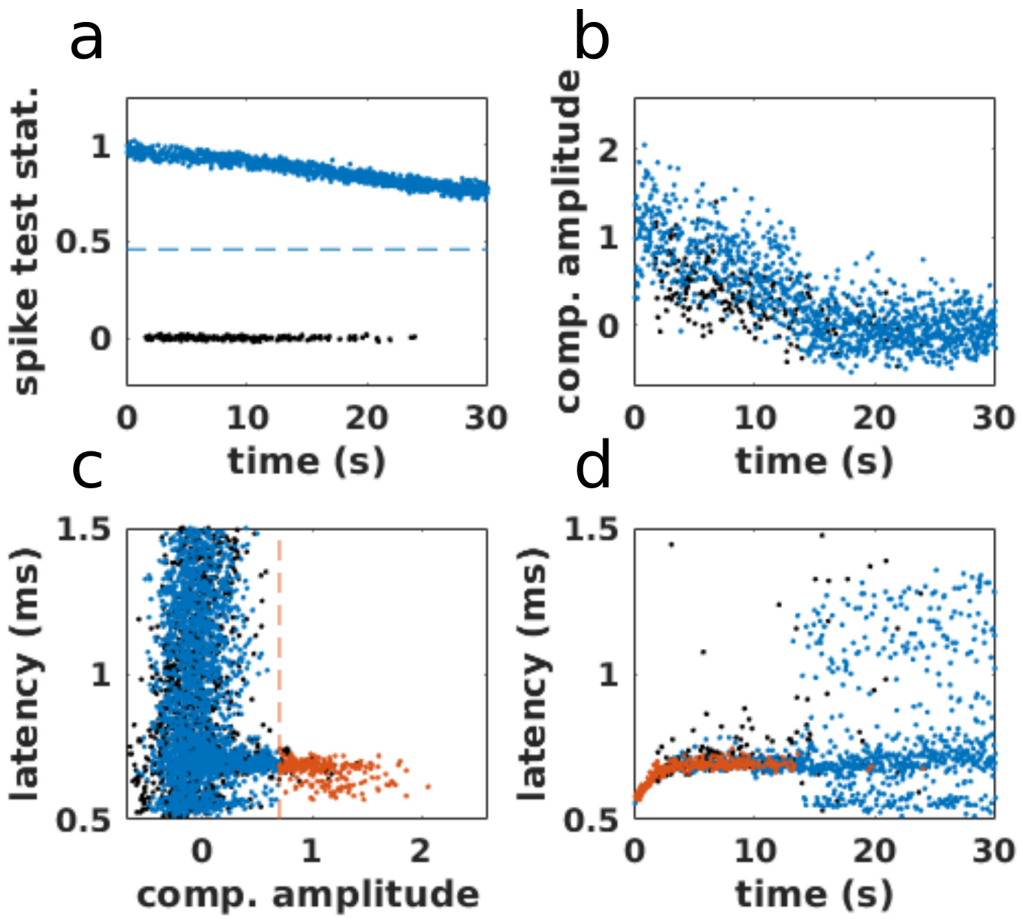

Figure 3.7: Template specific amplitude thresholds help to decrease artificially high latency variance estimates. *(a)* Spike detection performed with a test stat computed from the estimated amplitudes of each point along a propagation path. Note the wide margin between detected spikes (in blue) and trials without a response (black). *(b)* Amplitude of one compartment along the propagation path, shown for both trials with spikes (blue) and response failures (black). Note that though the amplitude of the compartment does decrease over time, the measured AP amplitudes overlap with amplitudes generated by noise along. *(c)* estimated compartment eAP latency versus estimated compartment eAP amplitude. Note that as eAP amplitude decreases, the distribution of estimated eAP latencies expands considerably, even when the spike detection test statistic crossed threshold. By further requiring that eAPs from this compartment must have an amplitude above a compartment-specific threshold (orange), we restrict analysis to eAP estimates which have a decreased likelihood of coming from false positives.

Biological sources of latency variance

For small enough axons, an action potential traveling along an axon will always have a small variance of propagation time due to the inherent stochasticity of ion channel openings[92]. For sequential segments of axon which are sufficiently long or far enough apart, this variance will be independent, meaning that the propagation delay along the total axon will have a variance equal to the sum of the variances of the constituent segments. As such, for a segment of axon with uniform ion channel density and diameter, propagation delay variance will be proportional to the length of the measured segment, and the coefficient of variation will be inversely proportional to the length of the measured segment. The Fano factor, however, will be independent of the measurement length, depending only on the biophysical properties of the axon.

In addition to ion channel stochasticity, propagation delays also vary due to activity-dependent slowing. Unlike propagation variance due to ion channel stochasticity, propagation variance due to slowing is expected to be correlated along the axon, with the entire axon showing increases or decreases in conduction velocity from trial to trial. For a segment of axon where spatially uniform changes in conduction velocity were the only source of latency variance, variance would be proportional to the square of the measurement length, and the coefficient of variation would be independent of measurement length.

Both stochastic jitter and correlated changes in conduction velocity occur in most experiments. These can be disentangled by calculating the first order difference between latencies. As propagation changes due to activity-dependent slowing tend to accrue gradually over thousands of trials, the mean change in delay from one trial to the next is quite small compared to the trial-to-trial jitter due to the inherent stochasticity of propagation. As such, the difference in latency between subsequent action potentials has a near zero mean, and a variance equal to twice the variance of the trial-to-trial variance. This provides a simple method of disentangling trial-to-trial variance from the variance associated with the gradual changes in latency due to activity-dependent slowing.

Latency variance from errors

A third source of variance in latencies of propagating action potentials is latency error. While jitter and conduction velocity changes lead to variance that increases along the propagation path, latency errors add to the variance of only a single latency measurement along that path. One hallmark of latency measurement errors, therefore, is a decrease in the variance along the propagation path.

Latency errors measured within a single experiment can easily vary by several orders of magnitude. The distribution of latency errors is dependent on the amplitude of the measured action potential. At some amplitudes, the error distribution is approximately Gaussian, while at others it has very long tails. With a low enough amplitude, latency errors can be treated as originating from a uniform distribution covering the entire available spike detection range.

Due to it's large amplitude, the expected error associated with measurement of AIS latency even with traditional spike detection mechanisms is roughly 3 μs[6]. As such, AIS latency variance provides an important measurement for setting bounds on biological variance. For antidromic propagation, it can be used to put an upper bound on the latency variance along the propagation path. The relative contribution of jitter and conduction velocity to the AIS latency variance can be estimated by calculating the variance of the first order difference, and making the simplifying assumption that jitter and conduction velocity variance are independent (note that there is evidence that this is not the case). This first order estimate of jitter and conduction velocity variance can then be used as a rough estimate of the expected variance at each recording location along the axon.

One approach to estimating latency variance in the presence of intermediate levels of error, is to use robust measures of spread, such as Median absolute deviation (MAD) and trimmed estimates of the variance. Median absolute deviation has the advantage of rejecting outliers even when they make up 50% of the available data, and without requiring any additional parameterization, the median being the logical end point of the trimmed

mean. However, the performance of the MAD diminishes when the variance being measured approaches the quantization level of the data, though this can be compensated for with upsampling.

3.6 Conclusions

While matched filters do greatly enhance the intelligibility of data collected on CMOS MEAs, the changes to AP waveforms which occur during activity-dependent slowing violate fundamental assumptions of their design and increase the difficulty of interpreting their results. Explicitly constraining estimated propagation times to follow a known propagation path does provide a flexible alternative to manual window setting, and means that every trial does have at least one coherent interpretation available. Note however that the presentation of this method is intended as a proof-of-concept, benchside view that this method does work and allows otherwise easily lost eAP waveforms to be detected and latencies estimated while introducing minimal biases into the process. The statistical model implicit within the method also offers the opportunity to predict performance based on template properties and to validate template accuracy. For now, these are left for future work.

Comparison of stimulation location introduces several biases into estimated propagation sequences, which must be carefully sifted through to minimize the impact of bias in the interpretation of the data.

While the iterative approach used for electrode and voltage selection described above was able to find sensitive stimulation sites relative quickly, it was not optimized to minimize cell-to-cell variation in stimulation reliability during the control condition. As mentioned in the methods section, measuring 10 out of 10 successful trials at 1 Hz did not guarantee continued reliability at 1 Hz stimulation for longer periods of stimulation, even at the same frequency. Stimulation screens must balance the cost of duration of the screen experiment, number of electrodes evaluated, stimulation frequency, and accuracy of the threshold estimates.

CMOS MEAs offer new insights into the cause of changing extracellular amplitudes associated with activity-dependent slowing. While in measurements of compound action potentials this change in amplitude can be attributed to changes in either the synchrony of the population response (due to changes in conduction velocity), or the reliability of the evoked responses, amplitude changes have also been reported for extracellular single-trial, single-axon recording methods [43]. With these methods, amplitude changes must be attributed to a change in the extracellular waveform, but the precise interpretation will depend on the filtering methods used. For the matched filters described above, any deviation in the extracellular waveform which does not alter the signal energy will cause a decrease in the calculated amplitude.

While we did not pursue methods to include waveform adaptation into these signal processing techniques due to the open-ended nature of predicting biological adaptation, there is one source of waveform adaptation that does warrant further investigation. Conduction velocity slowing itself unavoidably modulates extracellular action potential waveforms, while computational modeling has suggested impact on intracellular action potential waveforms may be quite small[29]. If conduction velocity slowing is the primary cause of waveform non-stationarity, rather than changes to the membrane current waveform, then the axonal action potential might still be detectable with the appropriate matched filter. Further, conduction slowing is a single dimension to describe adaptation, with constraints that can be set by the slowing literature (e.g., no more than twice and no less than 1/2 the resting conduction velocity).

Changing eAP amplitude and changing eAP width could be distinguished using more advanced filtering methods, including filter banks with different dilation correction factors and beamforming techniques. Distinguishing between waveform dilation and amplitude decreases for single trial AP recordings would serve a dual purpose of providing a more accurate picture of neural dynamics by gathering information on the instantaneous propagation velocity of the action potential at individual recording clusters, while also maximizing

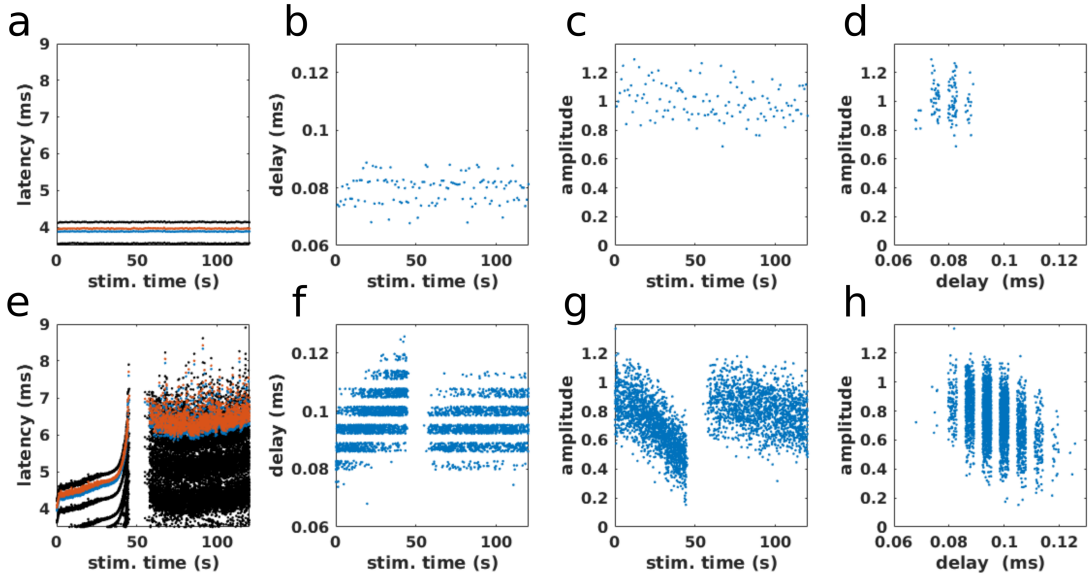

Figure 3.8: Correlation of matched filter amplitude and velocity. *(a)* Latency of eAP propagation in response to axonal stimulation at 1 Hz. Latencies of two sequential recording clusters are highlighted in blue and orange, responses on other clusters are in black. *(b)* delay between the two clusters highlighted in *a*. Jitter added for clarity, before jitter delays were quantized by an effective sampling interval of 6.25 μs. *(c)* sum of the amplitudes of the eAPs highlighted in *a*. *(d)* Amplitude versus delay. *(e-h)*, as *a-d*, to for responses to stimulation at 45 Hz. Note that delay and amplitude both deviate from their values measured at 1 Hz, and that delay is negatively correlated with amplitude.

signal strength in the face of common waveform distortions.

As propagation has a simple additive rule to describe how it works, it is in principle quite simple to create an estimator of true propagation time using a Kalman filter. Such an estimator can leverage initial estimates of variance due to slowing, jitter, and error in order to improve the accuracy of further measurements.

Future experiments may reduce the impact of misclassified spikes on this estimate by measuring propagation times at axonal locations orthodromic to the stimulation site, as well as antidromic. Regions orthodromic to the stimulation site would act as an independent measurement of initiation variability, helping to verify that initiation location does not change during repeated stimulation.

CHAPTER 4
IMPACT OF STIMULATION LOCATION ON ACTIVITY-DEPENDENT EXCITABILITY

4.1 Introduction

Individual electrical stimulation pulses produce reliable, well-understood effects in neurons. Repeated stimulation is much less well understood, however, as each stimulus-evoked action potential may modulate the responsiveness of the neuron to further stimulation. This activity-dependent excitability is especially apparent in small, unmyelinated axons with low resting firing rates, such as those found in cerebellum [39], hippocampus [25], or cortex [7].

Such stimulation-evoked activity-dependent excitability is of clinical interest, as there is evidence that clinical neural stimulation operates by engaging such processes. Li and colleagues showed that deep brain stimulation of the subthalamic nucleus for treatment of Parkinsons disease activates unmyelinated gray matter axons with roughly 30% reliability at 130 Hz, despite the same fibers being activated with $>$80% reliability at 10 Hz and below [20]. This frequency-dependent stimulation failure was responsible for the firing rate of stimulated neurons peaking in response to stimulation at 130 Hz, which is the same frequency that provided optimal symptom relief for the rats studied. Further, the unreliable nature of the axonal response to stimulation was shown to produce decorrelated activity in motor cortex, which may help to alleviate the pathological synchrony which characterizes Parkinsons disease.

The degree to which this activity-dependent excitability acts uniformly over different compartments within the same neuron is currently unclear. Modeling work [93] has showed a nearly identical increase in stimulation threshold for cell bodies and axons of

the spinal cord when stimulation frequency increased from 25 to 50 Hz, while showing non-monotonic effects of stimulation rate on the threshold of fibers of passage. Differences between the responsiveness of local axons and cell bodies were somewhat trivially widened through the use of extracellular waveforms that targeted one compartment or another. While the models used did include currents responsible for depolarizing after potentials, they acknowledged but did not include ion concentrations dynamics associated with elevated firing rates. Radivojevic and colleagues [46] recently reported experiments showing substantial variation in the number of action potentials that could be evoked by extracellular voltage stimulation at 100 Hz, using stimulation voltages that were reliable when used at 1 Hz. They generally found that the number of stimuli evoked in this way increased the closer they stimulated to the AIS. This suggests that stimulation at the AIS has a greater safety factor with respect to activity-dependent decreases in excitability than stimulation at the axon. However, by only stimulating at 100 Hz for 1 second, they limited the degree of engagement with activity-dependent processes that are activated by clinical stimulation protocols, which commonly stimulate chronically using pulses at 130 Hz or higher. Further characterization of how stimulus thresholds at different stimulus locations are impacted by activity-dependent excitability may help to clarify which neurons are activated during clinical neural stimulation, and the mechanisms involved in activity-dependent excitability.

In this chapter, we investigate how stimulation location alters activity-dependent changes in excitability in small unmyelinated axons. To do so, we stimulated and recorded from the axons of dissociated cortical cultures grown directly on top of high-density MEAs [61]. High-density MEAs enabled us to record action potentials at multiple locations hundreds of microns away from each other along single axons, with single-trial precision [67], which allowed stimulation failures to be distinguished from conduction failures [23] or failures of the AP to invade the soma [65].

4.2 Methods

To find stimulation voltages which reliably activated neuronal response at different parts of individual, synaptically isolated target neurons, stimulation electrodes were selected from the high density MEA at locations corresponding to either the axon or axon initial segment of the target neuron's AP footprint (Figure 4.1a). Stimulation threshold for voltage controlled, biphasic square waves (a 200 μs positive phase, followed by a 200 μs negative phase of equal amplitude) were then estimated at each of these electrodes through an iterative procedure. On each iteration, a stimulation amplitude was selected, starting with a positive phase of 500 mV. 10 stimuli of the chosen amplitude were then applied to each electrode individually, with an inter-stimulus-interval of 1 s. Responses to stimulation on the target neuron were counted up, and all stimulation electrodes that evoked 10/10 responses advanced to the next round with a new stimulation amplitude. The stimulation amplitude selected was up to the experimenter, but generally advances were performed in 100 mV increments if successful responses to stimulation were found, and a binary search between the current stimulation amplitude and the last amplitude with successful responses if not. This continued until the minimum stimulation voltage for the lowest-threshold electrode was identified, within 25 mV. In some cases, the identified minimum reliable stimulation voltage did not evoke a response at 100% reliability during subsequent 1 Hz stimulation, prior to the application of higher stimulation frequencies. In these cases, stimulation voltage was then increased until a new minimum voltage was found, but the stimulation electrode was not changed.

Minimum reliable stimulation amplitudes were used for all subsequent stimulation. Our stimulation protocol was designed based on a previous study examining the dynamics of activity-dependent excitability in cultured dissociated cortical neurons grown on traditional MEAs [7]. Following their work, stimulation was applied in 'epochs' of stimulation pulses at a fixed frequency, with each epoch lasting 120 seconds. 300 seconds of rest were in-

cluded between each epoch to allow the cell to recover. As response reliability has been reported to decrease above cell-specific stimulation frequencies, usually 5-20 Hz [7, 43], we chose to stimulate at 1 Hz to evoke responses 'at rest', and 45 Hz was used to evoke responses with activity-dependent response reliability. Stimulation over the entire experiment consisted of one epoch of 1 Hz stimulation for each stimulation location, followed by 6-10 epochs of 45 Hz stimulation for each location, and ending with one additional epoch of 1 Hz stimulation for each location, for a total of 16-24 epochs lasting a total of 112-175 minutes.

All statistical hypotheses reported in this chapter and the next (25 total) were performed post-hoc, using data collected from a single sample of 5 neurons. We used the Bonferroni correction to test for significant differences while keeping the familywise error rate to 0.05 (significance level at 0.0020).

All P-values for hypothesis tests were calculated in MATLAB [75]. Comparisons of central location were performed using 'paired' (single sample) tests, as each variable was measured from each neuron in the sample. Sample distributions for each variable were tested for normality prior to comparison (Lilliefors test, significance set at α = 0.05). Tests for normality were not included in the Bonferroni correction. If neither variable was found to deviate significantly from normal, a paired t-test was used. Otherwise, we used a Wilcoxon signed-rank test. To minimize the number of post-hoc tests performed, all tests were two-tailed unless a specific reference could be supplied to support one tail or another.

4.3 Results

4.3.1 Stimulation safety factor at axon does not predict safety factor at AIS

We found that while the minimum reliable stimulation voltage at 1 Hz had a higher sample mean at the axon (203 mV) than at the AIS (138 mV) in agreement with [46], though this was not significant (p = 0.1013, one-sided t-test, n = 5 neurons, see Figure 4.1b).

We found that while subsequent stimulation at 1 Hz did show a slight drop in response reliability (Figure 4.1, c), there was no significant difference across stimulation location ($p = 1$, two-sided Wilcoxon signed rank test, $n = 5$ neurons). As the responsiveness of the AIS was observed to be highly reliable at an elevated stimulation frequency in a previous study, [46], we tested for a similar result in response to 45 Hz stimulation. Surprisingly, we did not observe a significantly higher response reliability at the AIS compared to at the axon when stimulation frequency was increased to 45 Hz (Figure 4.1d, $p = 0.5687$, one-sided t-test, $n = 5$ neurons). We also did not observe a significant correlation between response reliability at the AIS and response reliability at the axon on the same neuron ($R = -0.4444$, Linear correlation coefficient, $P = 0.4534$ two-sided t-test).

The insignificant results described above suggested that the wide range in response reliability we observed was no due to different degrees of sensitivity to activity in different neurons, nor due to trends in the excitability of the axon and axon initial segment. We then attempted to see if it could be explained by features of our stimulation protocol. Due to the granularity of the stimulation voltage selection method we used, we checked if the stimulation voltage impacted reliability at 45 Hz. While there we found a slight negative correlation with stimulation voltage ($R = -0.31$, linear correlation coefficient), this was not significant ($p = 0.37$, two-sided t-test, $n = 10$ stimulation epochs, 1 epoch per stimulation site, 2 stimulation sites per neuron, see Figure 4.1e).

4.3.2 Decreased stimulation reliability was not associated with greater impact on AP amplitude

One possible reason for this difference in stimulation reliability across stimulation locations may be that evoked APs propagating in different directions have different effects on activity-dependent excitability. As activity-dependent changes in excitability are often associated with decreases in extracellular AP amplitude, we compared the decreases in axonal AP amplitude induced during stimulation at 45 Hz in the two stimulation locations (Figure

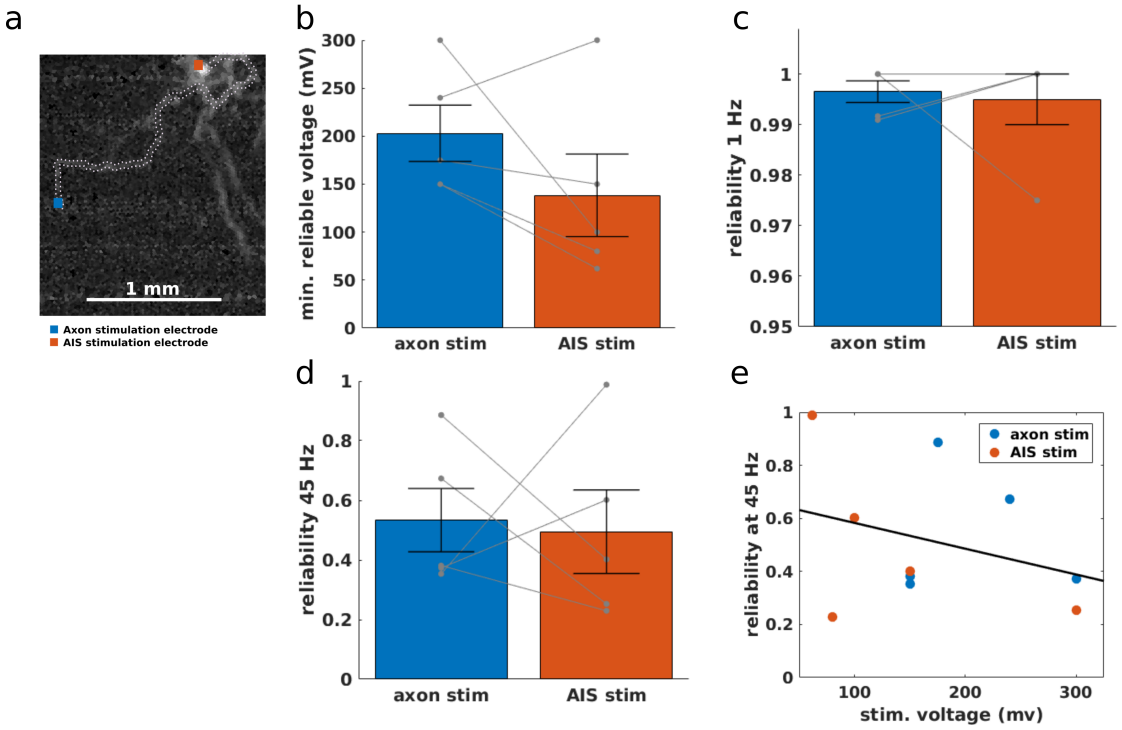

Figure 4.1: Comparison of response reliability across stimulation locations at 45 Hz. *(a)* stimulation pulses were applied at two different locations on synaptically isolated neurons located electrically on high-density MEAs. *(b)* minimum reliable stimulation voltage identified for each stimulation location on each neuron in this experiment. For each bar plot shown here, grey lines connect measurements from the same neuron, blue and orange bars show sample mean, and error bars show sample standard error of the mean. *(c)* Response reliability to the first epoch of stimulation at 1 Hz. Note that the vertical axis scaled for clarity. *(d)* Response reliability to the first epoch of stimulation at 45 Hz. *(e)* reliability at 45 Hz versus stimulation voltage. Linear fit of reliability to stimulation voltage shown in black, using data from both groups.

4.2). Extracellular AP amplitude was recorded at all electrode clusters where the eAP was not obscured by stimulation artifact during stimulation at either location, and normalized relative to the mean amplitudes measured on APs evoked during the control conditions (Figure 4.2b).

We find that mean eAP amplitude also decreases during stimulation at 45 Hz, and that there was also no significant difference across stimulation location ($p = 0.7603$, two-sided t-test, n = 5 neurons, Figure 4.2c). However, we do find that mean axonal eAP amplitude tends to decrease more when stimulation response reliability is high, and tends to show little deviation from control when stimulation response reliability is low (linear correlation coefficient = -0.65, $p = 3.411 \times 10^{-8}$ using Student's t-test, n = 60 epochs, with 6 per stimulation site, 2 stimulation sites per neuron, 5 neurons. See figure 4.2d). Note that this was also significant when evaluated for the two stimulation conditions separately (both with $p<0.001$, t-test, n = 30 epochs, 6 per neuron), but there was no significant difference between the two correlations ($p = 0.46$, using the difference of z-transforms on the correlation coefficients, t-test, n = 30 epochs, 6 per neuron). This suggests that the variation in reliability seen here is not due to a difference in how antidromic and orthodromic propagation impact activity-dependent processes at the level of the entire cell, but is instead due to how these activity-dependent processes impact local excitability at the AIS and axon.

We then compared the time course of changes in stimulation reliability over multiple stimulation epochs for both stimulation directions on each neuron (Figure 4.3.) While limited by the sample size of the study, we find that three neurons show an immediate drop in reliability down to roughly 0.5 during the first epoch of axonal stimulation at 45 Hz, and on subsequent epochs of 45 Hz show further decreases in reliability, reaching 0.1 reliability and lower. Despite this loss of responsiveness at 45 Hz, all of these neurons showed at least some response to subsequent stimulation at 1 Hz, though at reduced reliability relative to the initial control. In each of these cases, however, responsiveness to 1 Hz stimulation did increase in the second half of the subsequent 1 Hz stimulation, relative to the first half

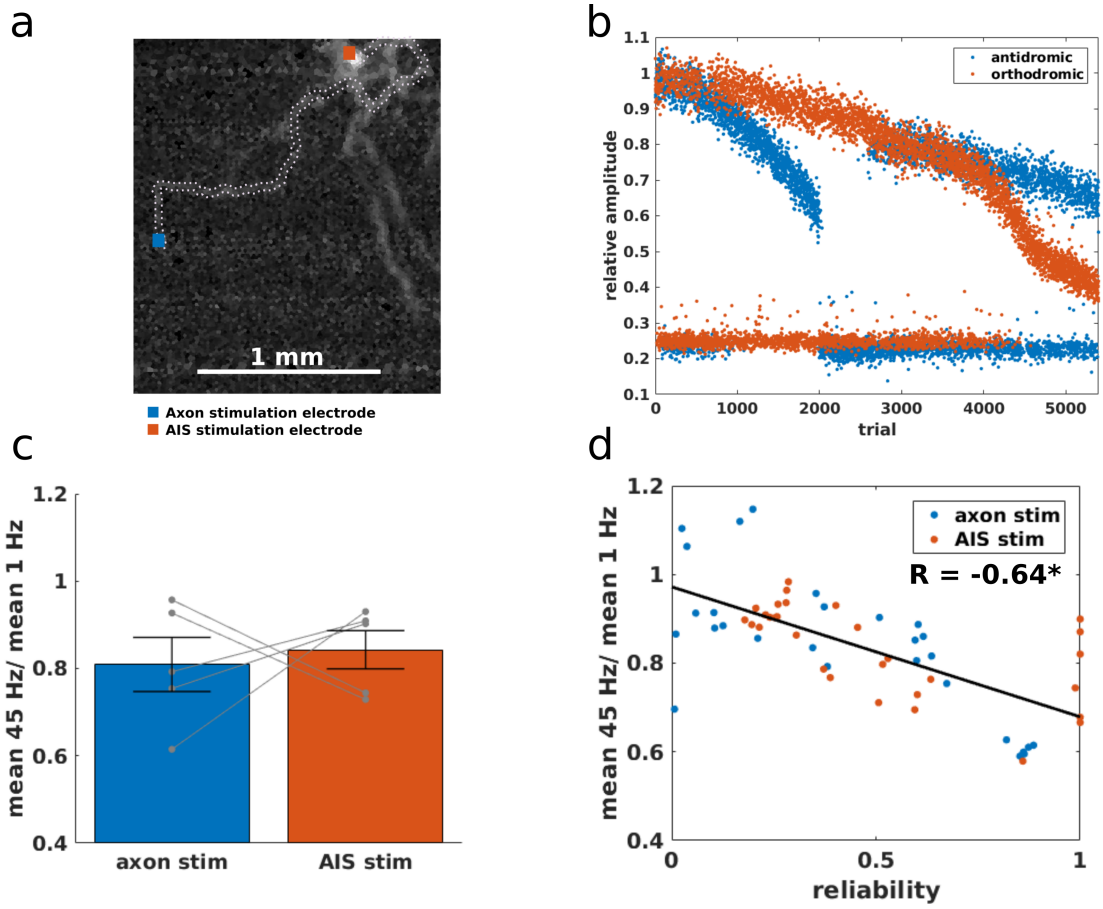

Figure 4.2: Decreases in axonal amplitude are associated with elevated stimulation reliability. *(a)* Amplitudes of axonal action potentials were measured in response to electrical stimulation at the axon and near the AIS. *(b)* Example data showing axonal AP amplitudes decreasing over the course of 45 Hz stimulation, for either stimulation location. Response failures are seen centered at amplitude = 0.25. *(c)* Mean amplitude of axonal APs measured in response to stimulation at 45 Hz on two different locations for each of 5 cells. Each cell is shown as a grey line. Bar plot and error bars show sample mean and sample standard error of the mean, respectively. *(d)* Mean axonal AP amplitude versus reliability of response to stimulation. Shown are 6 repeats of the two minute long experiment shown above, for each of 5 cells. Linear fit of amplitude ratio to reliability shown in black, using data from both groups. *p <0.002

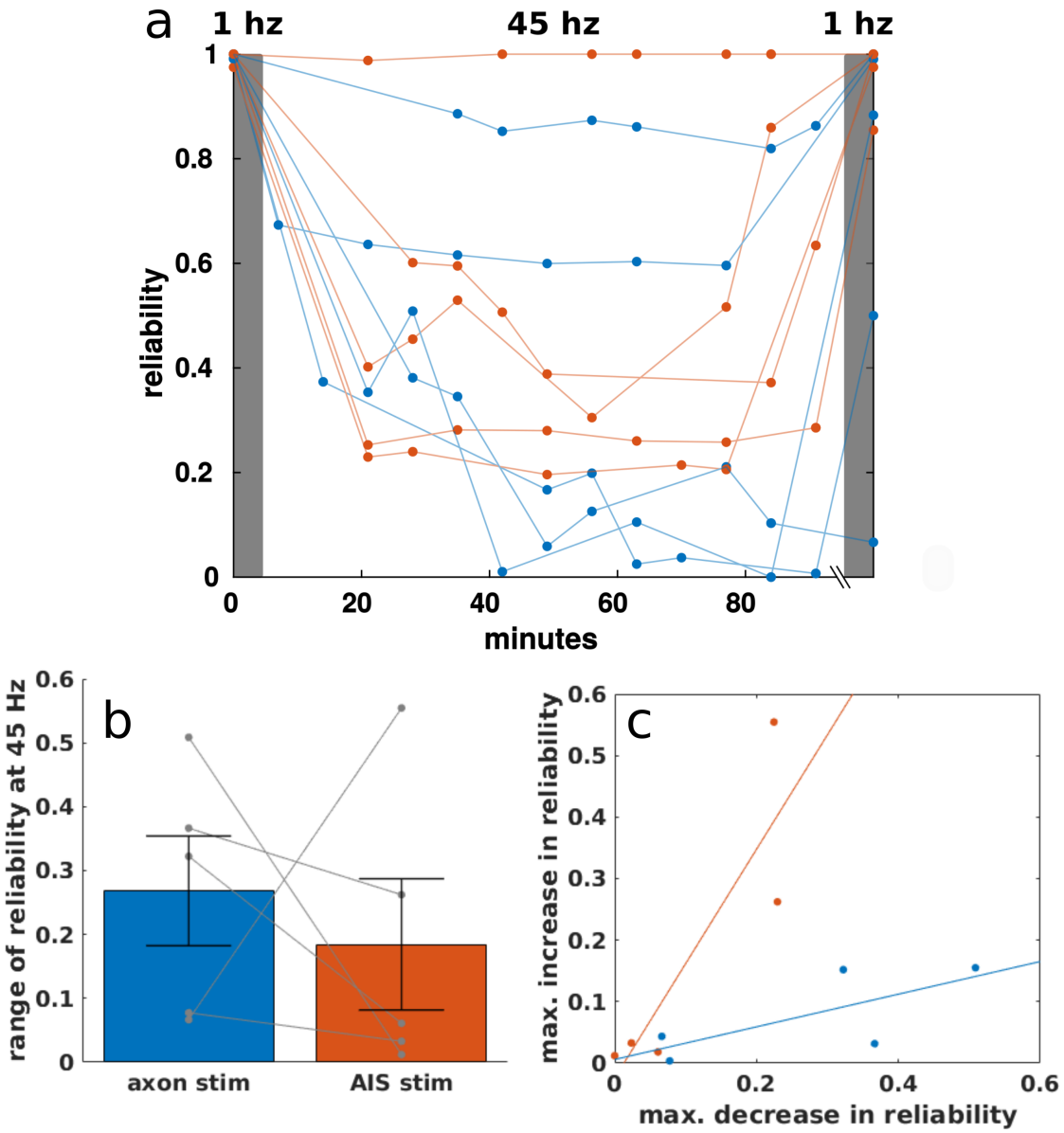

Figure 4.3: Comparison of stimulation reliability over epochs of stimulation applied at different stimulation locations. *(a)* Mean response reliability for responses to 120 second long epochs of stimulation at 1 Hz (grey background) and 120 second long epochs of stimulation at 45 Hz (white background). Data shown for 5-6 epochs of 45 Hz stimulation. As experiments varied in the total number of applied stimulation epochs, 1 Hz stimulation at the end of this sequence varied across experiments. Data from additional epochs were removed to show all neurons side by side. Epochs of axonal stim and AIS stim on the same neuron were initially interleaved and are aligned here relative to the first 1 Hz stimulation epoch for each electrode. Responses to axonal stimulation are in blue, responses to AIS stimulation are in orange. *(b)* The range of reliabilities measured at 45 Hz for each stimulation condition. Measures from the same cell are connected with a grey line. Bar plot and error bars show sample mean and sample standard error of the mean, respectively.*(c)* Maximum drop in reliability over 45 Hz epochs vs maximum increase in reliability over epochs. Responses to stimulation at the axon in blue, responses to stimulation at the AIS in orange. Trend lines are shown in each color.

(data not shown). This suggested that responsiveness may have recovered further had the experiment continued longer. Further, in all three cases no drop in the amplitude of eAPs measured closest to the stimulation site showed changes in amplitude when measured in response to AIS stimulation (data not shown). In the two other axonal stimulation cases, stimulation response reliability never decreased below 0.6, and reliability of the first and last epoch did not differ by more that 0.1.

Interestingly, response reliability for stimulation near the AIS did not show this same drop in reliability over consecutive epochs, even in cases where reliability dropped to as low as 25% on the first stimulation epoch. While there were two cases where the reliability of response to AIS stimulation did vary by 0.2 or more during sequential stimulation epochs, both of these cells showed large (> 0.2) increases in AIS stimulation response reliability, which was not observed for axon stimulation. This demonstrates that response reliability at both the axon and the AIS are in some cases stable over 90 minutes. It also suggested that the dynamics of response reliability may be dependent on stimulation location, with a greater capacity for recovery of excitability when stimulating near the AIS. We attempted to quantify this stability using the range (maximum - minimum) of response reliabilities measured during epochs of 45 Hz stimulation. Reliability range did not show a significant difference between stimulation at the axon and axon initial segment ($p = 0.6343$, two-sided t-test, $n = 5$ neurons. See Figure 4.1b). This suggested that stimulation location did not determine the degree of consistency of response over multiple stimulation epochs, and that both consistent (small range of reliabilities) and inconsistent (higher ranges of reliability) response was possible at both stimulation locations. To quantify possible differences in the types of dynamics in stimulation response, we examined the degree to which stimulation response reliability would show both increases and decreases over epochs.

4.4 Discussion

We find that stimulation reliability at 45 Hz decreases at both the axon and the AIS, relative to stimulation at 1 Hz using the minimum reliable stimulation voltage as found at 1 Hz. This reliability change is not consistent across stimulation locations or across individual cells, though for both stimulation locations the number of evoked APs was well correlated with decreases in the extracellular AP amplitude. Additionally, we find instances of stable response reliability, which does not change by more than 0.1 over 90 minutes, as well as instances where response reliability either dropped nearly to zero (for some cases of axonal stimulation), or showed decreases and increases in reliability over epochs (for some cases of AIS stimulation).

We were surprised to find that stimulation at the AIS was not consistently more reliable during 45 Hz stimulation than that at the axon. Stimulation threshold at rest is lower at the AIS than at the axon proper [94]), due to the density and specialized sub-types of voltage gated sodium channels in the AIS [95]. In [46], a similar experiment to that shown in Figure 4.1 was performed on 4 neurons in dissociated cortical cultures grown on high-density MEAs, stimulating at both the axon and the AIS at 100 Hz for 1 second using super-threshold pulsatile stimulation. They find near 100% reliability when stimulating the electrode which recorded the first peak during a spontaneous action potential on the stimulated neuron, and roughly 50% reliability when stimulating the distal axon (see their Figure 8). We find near 50% reliability when stimulating for a single epoch near both the AIS and distal axon, using a lower stimulation frequency (45 Hz) but applied for a longer period of time (120 seconds). When examined over repeated epochs, a larger difference between mean axonal (0.40) and AIS (0.50) stimulation response reliability was observed, and restricting our analysis to only the first second of stimulation on each epoch showed a reliability of 0.76 for AIS stimulation and 0.62 for axonal stimulation (data not shown), somewhat tightening the gap between our results and those reported by Radivojevic and

colleagues, though our results still show substantially lower reliability for AIS stimulation compared to their reported reliability of nearly 1.0. This may be due to the small sample size of the two studies, though there are two important methodological differences to consider as well. First, the stimulation protocol used in [46] differs in total mean stimulation rate (9.09 Hz compared to our 12 Hz), which may have altered the recruitment of activity-dependent changes in excitability they report. Secondly, we also distinguish between the somatic or AIS action potential, and the action potential of the axon. The somatic action potential is known to have a longer refractory period than the axonal action potential [65], so it is possible that the relatively lower reliability of axonal stimulation observed in [46] is due to failures of somatic invasion, rather than failures to evoke an action potential in the axon.

The fact that we find a strong correlation between induced eAP amplitude and the number of evoked spikes suggests that changes in neural excitability must be examined at a very local scale to identify the mechanisms which drive stimulation reliability in response to repeated stimulation. This will require a careful control of stimulation voltage and distance relative to the axon. The granularity of stimulation voltage selection used here, at 25 mV, is a likely source for the variability in response we see in reliability. Stimulation electrodes with a larger stimulation voltage relative to the true threshold would be expected to respond more reliably, for longer periods of time. Distance relative to the axon was also not accounted for in electrode selection, and it is possible that differences there may in turn lead to differences in the length of axon which stimulation engages with, with possible consequences for the resilience of stimulation to activity-dependent excitability.

While the limited sample size in this study prevents strong generalizations about classes of neural response to stimulation, the trends observed in the dynamics of stimulation responsiveness at 45 Hz at different stimulation locations are suggestive of different mechanisms of activity-dependence of response. There are several mechanisms that may be responsible for activity-dependent changes to excitability [3]. Due to the fine diameter of

unmyelinated cortical axons (0.4-1 μm), intracellular sodium concentrations may increase during periods of high firing rate[32], with larger branches and the soma remaining relatively untouched. This location-dependent change in the sodium Nernst potential would be expected to translate to differences in stimulation threshold.

An interesting consequence of these differences in reliability is that while blind stimulation of neurons is generally believed to activate axons preferentially over cell bodies, axonal stimulation may not show the same staying power as AIS stimulation. This may in turn mean that at the stimulation frequencies used in clinical neural stimulation (often 130 Hz or greater), cell bodies are the most reliable responders.

CHAPTER 5

INITIATION DELAY CONTRIBUTES TO AP LATENCY DYNAMICS

5.1 Introduction

In the previous chapter, we showed that response to repeated electrical stimulation at 45 Hz is dictated by local, rather than neuron-wide excitability dynamics. This finding is surprising, considering that decades of experiments in a variety of preparations ([27, 39, 25] for reviews, see [3, 22]) have demonstrated that activity-dependent changes in stimulation threshold are mirrored by changes in conduction velocity. Altering conduction velocity requires distributed changes throughout the axonal arbor, rather than local to the site of stimulation. This distinction suggests that response to repeated electrical stimulation which induce intermittent response failures[7] are determined by a distinct set of dynamics from those which alter conduction velocity.

Confirmation of this hypothesis through direct measurements is hampered by the fact that as electrical stimulation is performed at voltages orders of magnitude larger than extracellular APs, necessarily obscuring their responses in the local axon. Local excitability can be monitored indirectly, however, through measurement of AP initiation delay[96]. Stimulus-evoked action potential times include contributions from propagation delay along the axon, as well as the time to initiate an action potential in response to stimulation (Figure 5.1). Near stimulation threshold, the mean and variance of initiation delay have been observed to increase as stimulation voltage decreases [67, 96], reflecting the inherent stochasticity of response to stimulation. Importantly, these changes are observable at some stimulation voltages which produce reliable responses [67], and can therefore be tracked prior to the occurrence of stimulation failures. However, it is not clear how initiation delay is modulated by activity, or the degree to which measurements of neural response latency to

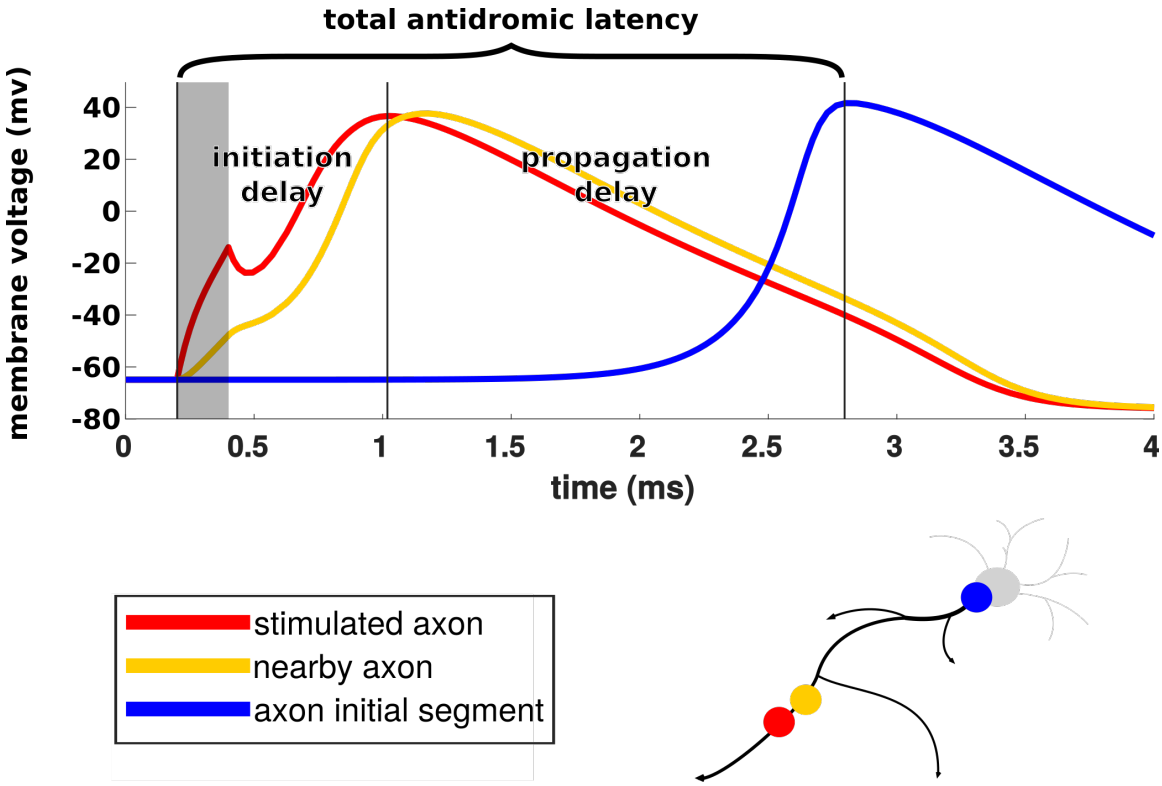

Figure 5.1: Sources of recorded latency in stimulation-evoked eAPs. Top: membrane potential of a simulated multicompartment Hodgkin-Huxley neuron model. Intracellular current is injected into one axonal compartment, leading to action potential initiation. The action potential, once initiated, then propagates to other compartments.

stimulation may be due to initiation delay in the presence of intermittent response failures [7].

To test if initiation delay is activity-dependent, we measured propagation times of action potentials evoked by electrical stimulation in small unmyelinated axons grown in culture. Small unmyelinated axons are generally more sensitive to repeated stimulation than larger cells, showing slowing at stimulation rates near physiological firing rates [25]. To distinguish between propagation delay and initiation delay we recorded axonal action potentials from neural cultures grown directly on top of high-density microelectrode arrays [61]. High-density MEAs allowed us to record action potentials at multiple locations hundreds of microns away from each other along single axons, with single-trial precision [67]. This single-trial precision enabled us to measure both the mean and variance of propagation

time, and to estimate initiation time.

5.2 Results

We measured the latency between stimulation and stimulus-evoked antidromic action potentials recorded extracellularly at multiple locations along the axonal arbors of 5 neurons grown in vitro. Propagation delay was estimated by subtracting spike latencies measured earlier in the propagation sequence from those measured later. Initiation delay was not measured directly in these experiments. Instead, the latency measured at the first usable compartment following stimulation was used as a proxy. This measurement, which will be referred to as initiation delay for brevity, contains a combination of propagation delay and true initiation delay. Time for the action potential to invade the AIS was estimated using the delay between the measured latency at the last measurable axonal compartment and the latency of the AP at the AIS.

5.2.1 Mean of first recorded latency of intermittent response to stimulation increases more than propagation delay

We found that the mean latency measured during stimulation at 45 Hz increased relative to 1 Hz for all measured initiation and propagation delays (Figure 5.2). Further, we found a greater increase in mean initiation delay relative to propagation delay in response to axonal stimulation, though this was not significant after correcting for multiple comparisons ($p = 0.0068$, one-sided t-test, $n = 5$ neurons. See Figure 5.2d). We similarly found that mean initiation delay increased more than propagation delay in response to stimulation at the AIS, but this was also not significant ($p = 0.0938$, one-sided Wilcoxon signed-rank test, $n = 5$ neurons. See Figure 5.2e). Both tests performed against the null hypothesis that initiation delay was less than or equal to propagation delay.

When comparing the first 45 Hz epoch on each cell, outliers due to false positive spikes were removed by manually setting an AP amplitude threshold for each recorded axonal site.

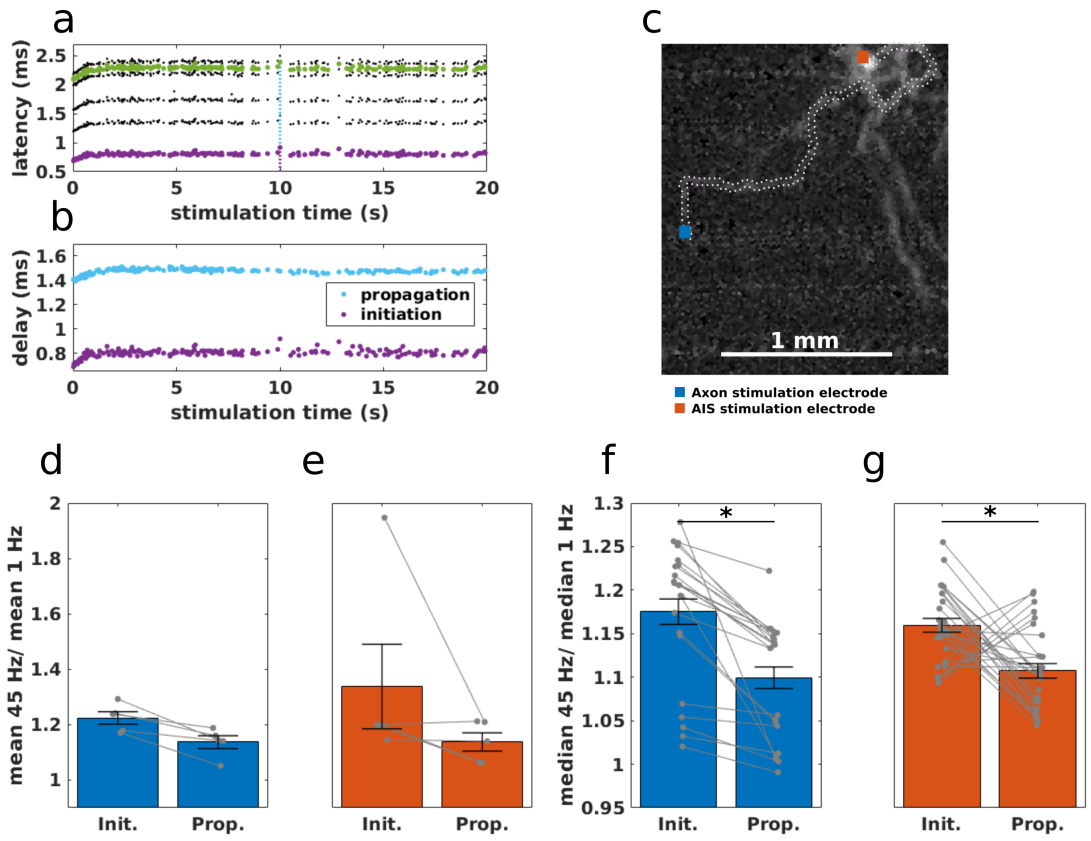

Figure 5.2: Larger relative increase for initiation delay than propagation delay during 45 Hz stimulation. *(a)* Small variations in latency at the first recorded location of an AP (purple) were often seen to be present at all subsequent compartments (black). *(b)* Measuring delay between compartments shows propagation delay (cyan) which is may have qualitatively distinct features from initiation delay. *(c)* Initiation and propagation were measured in response to stimulation near the axon (blue) and AIS (orange). *(d)* Mean latency of initiation and propagation delays measured at the first 45 Hz epoch in response to axonal stimulation and *(e)* AIS stimulation. Latencies were normalized by dividing by mean latency measured during 1 Hz stimulation. All bar plots show sample means and sample standard error of the mean. *(f)* median latency of initiation and propagation delays measured at for 6 stimulation epochs applied to each of 5 cells, measured in response to to axonal stimulation. *(g)* The same, measured in response to AIS stimulation . *p$<$0.002

For analysis of all epochs, the same AP thresholds were used to minimize false positives, but in most cases a few false positives (less than 5% of trials) remained. Median latency was therefore used for analyses of the entire set of epochs to mitigate the impact of these false positives. This trend was robust to the changes in stimulation reliability which occurred over repeated epochs of stimulation on the same neuron for stimulation at the axon (Figure 5.2f, p = 2.1506 x10^{-5}, one-sided Wilcoxon signed-rank test, n = 30 epochs, 6 epochs per neuron) and AIS (Figure 5.2g, p = 4.8929 x10^{-4}, one-sided t-test, n = 30 epochs, 6 epochs per neuron). Both tests performed against the null hypothesis that initiation delay was less than or equal to propagation delay.

5.2.2 Variance of first recorded latency of intermittent response to stimulation increases more than propagation delay

Latency variance also increased for all nearly all measured delays, when stimulation was increased to 45 Hz (Figure 5.3). Axonal stimulation caused an increase in initiation delay (Figure 5.3a, p = 0.0060, one-sided t-test, n = 5 neurons) and propagation delay (Figure 5.3b, one-sided p = 0.1053, t-test, n = 5 neurons). Similar increases were seen in in response to AIS stimulation for initiation delay (Figure 5.3c, p = 0.0410, one-sided t-test, n = 5 neurons) and propagation delay (Figure 5.3d, p = 0.1149, one-sided t-test, n = 5 neurons).

To compare initiation and propagation delay variance measured on the same axon, we computed their Fano factor. Fano factor of initiation delay was not significantly larger than the Fano factor of propagation delay at 1 Hz for either axonal stimulation (Figure 5.3e, p = 0.7812, one-sided Wilcoxon signed rank test, n = 5 neurons) or AIS stimulation (Figure 5.3f, p = 0.4062, one-sided Wilcoxon signed rank test, n = 5 neurons). However, when stimulation frequency was increased to 45 Hz, initiation delay surpassed propagation delay for both axonal stim (Figure 5.3g, p = 0.0114)and AIS stim (Figure 5.3h, p = 0.0312, one-sided Wilcoxon signed rank test, n = 5 neurons).

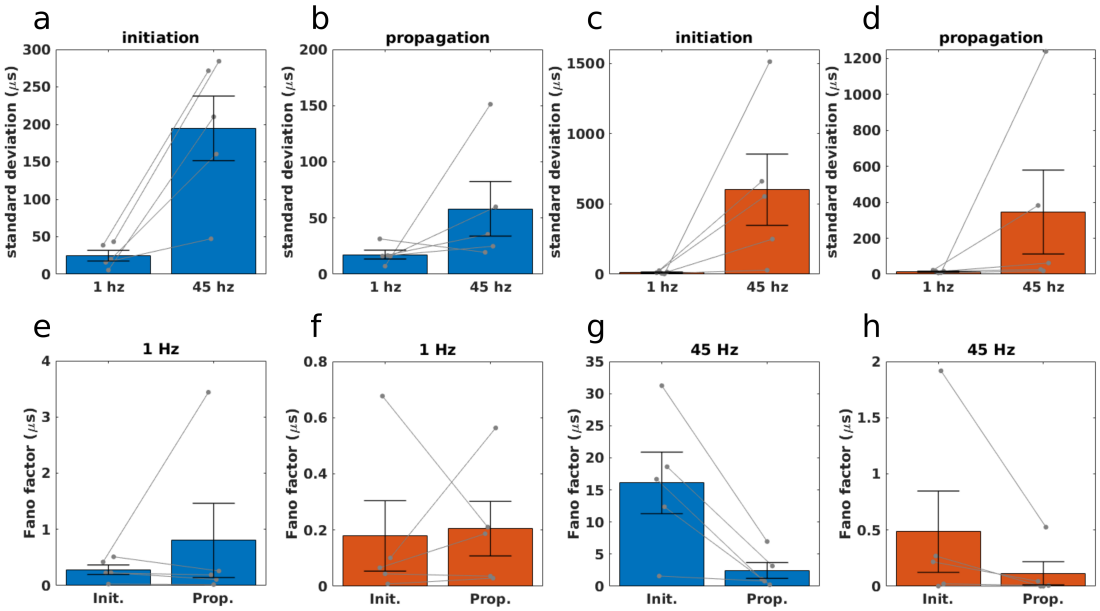

Figure 5.3: Standard deviation increases for all delays, but Fano factor increases more for initiation than propagation. *(a)* Standard deviation for initiation after axon stimulation, *(b)* propagation after axon stimulation, *(c)* initiation after AIS stimulation and *(d)*propagation after AIS stimulation. To compare latencies measured at different locations along the axon, variances were normalized by calculating the Fano factor. *(e)* Axon stimulation at 1 Hz. *(f)* AIS stimulation at 1 Hz. *(g)* axon stimulation at 45 Hz. *(h)* AIS stimulation at 45 Hz. All bar plots show sample means and sample standard error of the mean.

5.2.3 No conclusive difference in activity-dependence of first recorded latency and propagation delay

We then examined the impact of stimulation reliability on initiation and propagation delay (Figure 5.4). Median initiation delay increased with stimulation reliability (Figure 5.4b, R = 0.4067, p = 0.0028, two-sided t-test, n = 60 epochs), as did median propagation delay (Figure 5.4c, R = 0.4624, p = 5.5763x 10^{-4}, two-sided t-test, n = 60 epochs), with no significant difference between their correlation coefficients (p = 0.73, using difference of z scores). Fano factor was estimated using MAD^2/median for correlation analysis with reliability. The estimated Fano factor of initiation latency showed a slight negative correlation with reliability, though this was not significant (Figure 5.4d, R = -0.0785, p = 0.5582, two-sided t-test, n = 60 epochs). For propagation delay, estimated Fano factor showed a slight positive correlation with reliability, though this was also not significant (Figure 5.4e, R = 0.1916, p = 0.1497, two-sided t-test, n = 60 epochs).

5.3 Discussion

5.3.1 Evidence for activity-dependent initiation delay

Median latency was measured in 22 epochs of axonal stimulation and 30 epochs of AIS stimulation. 8 axonal stimulation epochs had a reliability of zero and therefore latencies could not be measured. Median delay increases were greater for initiation delay than propagation delay in all 22 axonal stimulation epochs and in 23/30 AIS stimulation epochs.

As each neuron studied differed in the length and geometry of its axonal arbor, as well as the relative signal strength of the axon throughout the arbor, the distances between recording locations differed across neurons. However, in the experiments reported here we did not acquire morphological data to measure the actual propagation distance. We used the Fano factor rather than coefficient of variation as a normalized metric of delay variance, following recent work suggesting propagation delay variance (and not it's standard

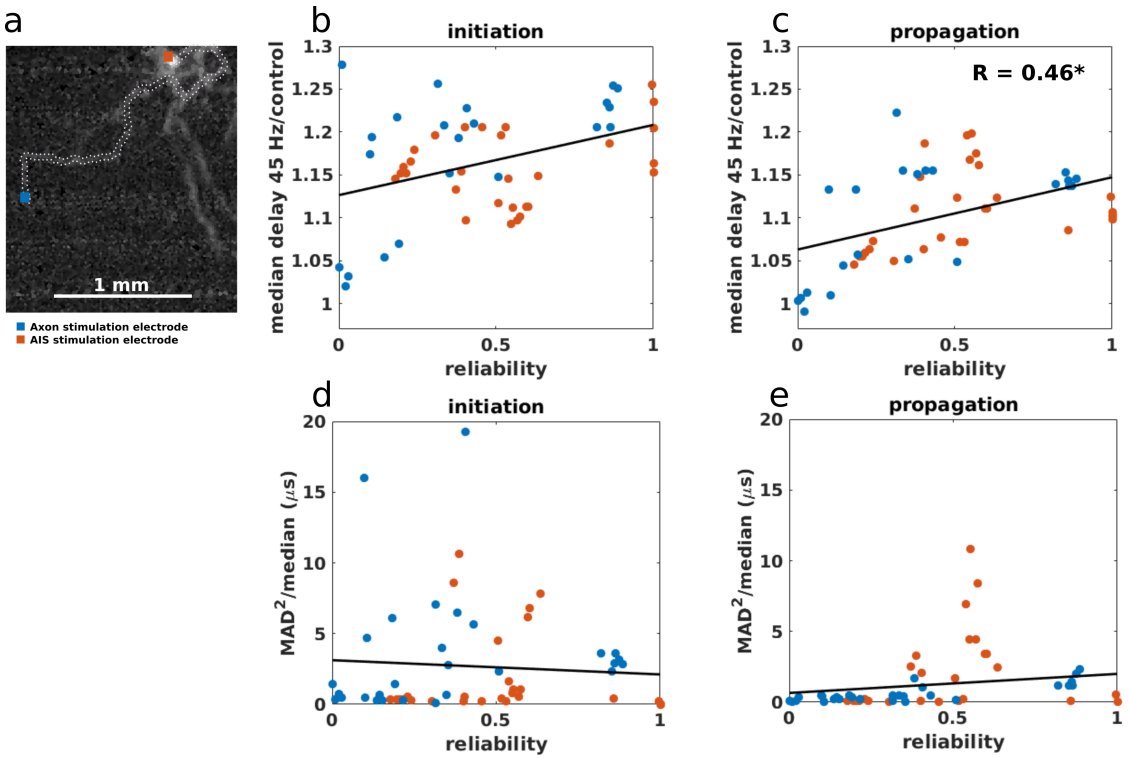

Figure 5.4: Initiation and propagation delays increase with increased stimulation reliability. *(a)* initiation and propagation delays were measured in response to 45 Hz stimulation at the axon (blue) and AIS (orange). *(b)* Median initiation delay and *(c)* median propagation delay increased at elevated stimulation reliabilities, for both axonal stimulation (blue) and AIS stimulation (orange). All delays were normalized to the median delay measured during the first epoch of stimulation at 1 Hz. *(d)* Fano factor of initiation delay and *(e)* propagation delay were estimated using the square of the median absolute deviation, divided by the median. This estimate of the Fano factor did not show consistent changes across stimulation reliability. Trend lines shown in black show the linear fit to reliability. *p<0.002

deviation) is proportional to propagation delay [67].

In the axonal stimulation experiment, an increase in Fano factor could also be explained by an increase in propagation variability of the distal axon relative to the proximal axon. During these experiments, the stim-sequent latency includes propagation within the most distal regions of axon recorded. Distal axon may be thinner than proximal axon, and therefore potentially more sensitive to the intrinsic stochasticity of ion channel state changes [92]. The lower volume of the distal axon would also make it more sensitive to some putative mechanisms of activity-dependent conduction slowing, such as intracellular sodium accumulation [32]. Again, the fact that we see the same trends in Fano factor of orthodromic propagation when stimulating near the AIS condition suggests that initiation delay itself increases the variance of the stim-sequent latency.

Variance in the stim-sequent latency could also increase due to changes in initiation location, rather than initiation delay. This differs importantly from initiation delay in that a change in initiation location will have opposing impacts on antidromic and orthodromic spike latencies, while a change in initiation delay will impact both antidromic and orthodromic latencies equally. Unfortunately the experiments we did here were not able to distinguish between these possibilities, but future studies of initiation time in the axon may be able to do so.

5.3.2 Biological significance

The activity-dependence of initiation delay are a fairly unexplored region of study that may play a unique part in determining the stochastic response to super threshold stimulation at frequencies higher than the axon can follow. By definition, initiation delay affects both antidromic and orthodromic propagation equally, in contrast to propagation delay which may differ for the two directions. Initiation delay is necessarily a more local process than the distributed process of propagation, which may translate to a differences in its sensitivity to some mechanisms. For instance, if any stimulation-evoked propagation failures occur,

they would introduce a mismatch in the number of action potentials fired in each part of the axonal arbor, and therefore possibly a mismatch in the recruitment of activity-dependent changes to excitability. The site of AP initiation within the axon would necessarily fire the most APs in this situation, suggesting that the AP initiation site may be uniquely modulated during periods of elevated stimulation frequency.

The changes in AP initiation delay seen here may be explainable as a natural result of known changes in stimulation threshold [25] interacting with near-threshold initiation delay variability. Both the mean and variability of AP initiation delay are known to increase when stimulating near stimulation threshold or at amplitudes that evoke less than 100% reliability relative amplitudes well above stimulation threshold [67, 96], though such measurements are usually made at control stimulation frequencies (such as 1 Hz) while varying stimulation voltage. This may be due to lower stimulation amplitudes initially recruiting a smaller mean number of voltage gated ion channels, increasing the variability of the spike initiation process. During this experiment, stimulation voltage was kept constant, but the stimulation reliability had decreased relative to what was seen at 1 Hz. Such decreases have been attributed to a variety of mechanisms, such as increases in intracellular sodium or slow inactivation of sodium channels. Many of these mechanisms would be expected to reduce the mean number of voltage gated sodium channels recruited by extracellular stimulation (such as those which decrease the voltage that the stimulated compartment is raised to, or decrease the number of available sodium channels), suggesting that this activity-dependent increase in initiation variance is an example of the same fundamental phenomena seen with voltage-dependent increases in initiation variance. Some putative mechanisms of changing stimulation reliability, which act by decreasing the impact of open sodium channels rather than the number of opened channels, may instead act in a manner distinct from the mechanisms of voltage-dependent initiation. For example, such mechanisms may preferentially increase mean initiation time over the variability of initiation time.

CHAPTER 6

DISCUSSION

We have shown that unlike the 'mirrored' changes in activity-dependent conduction velocity and stimulation threshold which occur during reliable stimulation [3], conduction velocity and reliability diverge from each other once response to stimulation becomes intermittent, as commonly observed during clinical neural stimulation[20, 19, 97]. In particular, conduction velocity is determined by the number of action potentials which travel throughout the cell. Stimulation reliability appears to be impacted by this, but is also dependent on other history dependent factors. This is in stark contrast to the decades of experimental observations that activity-dependent changes in stimulation threshold are mirrored by changes in conduction velocity. We further show that the local excitability changes manifest as changes in initiation delay, which introduces additional variance in neural response latency than would be expected by propagation delay alone. A consequence of this is that conduction velocity is determined by stimulation reliability, rather than providing an independent measurement of excitability which might be able to predict stimulation reliability.

Establishing that excitability dynamics are local, while propagation dynamics are cell-wide, still leaves many questions unanswered: *what* dynamics? What local biophysical state variables- ion concentrations, channel states, voltages- are engaged by intermittent response failures? And how are these impacts constrained to a local region for stimulation?

One explanation of the origin of this local change in excitability is propagation failures induced by regions of low safety factor. If stimulation-evoked action potential propagation throughout the axon arbor is throttled by propagation failures at a particular branch point, for instance, then we would expect that the region between the site of AP initiation and the branch point would be the region most impacted by this activity. Stimulation of this axon site would then involve interactions between evoked APs, their refractory periods, and even

possible reflections off of the point of low safety factor itself. Firing rate measured through the axonal arbor becomes less of an indicator of the reliability of response to stimulation, and more of an indicator of the number of APs which the low safety factor region passes. If this is the case, it is surprising how quickly propagation encounters a point of low safety factor in the propagation paths we measure here.

6.1 Implications for clinical neural stimulation

6.1.1 AIS stimulation may produce more APs than axonal stimulation during chronic stim

We demonstrate cases where stimulation reliability at the axon, but not at the AIS, dropped rather drastically at elevated stimulation frequencies. We may cautiously consider that if repeated, this result would suggest that axonal stimulation does not have the same 'staying power' as stimulation near cell bodies, with implications for the targets of deep brain stimulation. Three neurons showed an extremely slow decay (time constant estimated to be roughly 30 minutes) of reliability over epochs when their axons were stimulated at 45 Hz, and did show at least partial recovery of stimulation reliability at subsequent 1 Hz stimulation. Little can be concluded from this observation on it's own, especially without additional measurements to confirm that this change was actually induced by the increased stimulation frequency. However, it is unclear what mechanisms could be responsible for such a slow drift in excitability. Cellular movement is unlikely, considering that the axonal action potential could still be recorded during orthodromic propagation. It is possible that these neurons were already transitioning to a 'silent' state, which was accelerated by a brief period of elevated activity. Non-spiking neurons which are unresponsive to sensory stimulation are often found in cortex, where they are hypothesized to act as a "plastic reserve" in case their more active neighbors die off or sensory stimulation increases [66]. Interestingly, conduction delays of these inactive neurons are longer than active cells [66]. Previous work on high-density MEAs has shown correlation between the spontaneous firing rate of a neu-

ron and it's resilience against activity-dependent slowing effects [43].

If the grouping that we see holds up with additional measurements, it may imply a cell-type specific impact of DBS, with quiet or weakly spiking cells being removed from the circuit while more robustly active cells are able to continue.

6.2 Implications for the physiology of small unmyelinated axons

Our results suggest that repeated antidromic and orthodromic propagation have very similar effects on activity-sensitive features of propagation, such as changes in extracellular AP amplitude. This implies that the mechanisms of activity-dependent slowing are impartial to propagation direction-ie, that an antidromic spike causes as much slowing as an orthodromic spike, rather than showing more slowing in response to unnatural antidromic propagation. This is somewhat surprising as axon morphology is expected to cause to differences in the safety factor of propagation for the two propagation directions. Axons are expected to decrease in diameter as they travel away from the soma, up till some point at which diameter reaches a steady state. Orthodromic AP propagation therefore travels in the direction of generally decreasing diameter, which improves the safety factor of propagation, assuming constant ion channel densities along the axon. Reversing the propagation direction inverts geometric ratios, and would be expected to cause a decrease in propagation reliability during antidromic propagation. This difference in safety factor can delay propagation, leading to wider aps which may cause larger shifts in intracellular ion concentrations. The fact that we see no significant difference between the correlation of firing rate and amplitude changes for antidromic and orthodromic propagation suggest that these differences may be quite minor in our neurons.

6.3 Implications for timing codes

Our results suggest that measurement of antidromic latency changes with intermittent response failures may include contributions from initiation delay within the axon, which do

not reflect excitability dynamics of spike generation at the AIS. However, the changes in propagation latency which occur during intermittent responsiveness are qualitatively similar to those observed in measurements of activity-dependent slowing during reliable stimulation in a variety of preparations [98, 26, 25]. This suggests that measurement of activity-dependent slowing with stimulation frequencies which are low enough to reliably evoke a response are sufficient to predict how slowing will impact spike timing.

This suggests that activity-dependent slowing has minimal impact on spike timing. The degree of propagation slowing we report here, roughly 40% increase relative to conduction at rest (see Figure 5.2), fits with previous measurements of activity-dependent slowing [98, 25]. A 40% increase in conduction time would have negligible impact on 'driver' type neurons [99], which tend to have short conduction delays at rest. The much longer conduction delays associated with 'modulator' type neurons (up to 40 ms) may be expected to change by a substantial margin, however the longer time constants of the synapses associated with these neurons suggest that their spike timing may not be as relevant to computation.

One exception to this may be that branch points cause activity-dependent modulation of timing in at levels above standard activity-dependent slowing curves. While in most experiments, latencies were qualitatively similar along the propagation path, there were some notable exceptions for both antidromic and orthodromic responses. However, the distinct qualitative dynamics seen in the neurons included in this study prevented anything more than a series of n=1 investigations on the subject. As branch point failures are expected to occur early in the propagation path, it is possible that some of the variance in initiation latency which we report here may be due to branch point failures which were obscured by stimulation artifact. Teasing branch point failures apart from other types of response failures, such as those caused by ion channel stochasticity, will require additional characterization of these simpler mechanisms of initiation failure.

The locality of these excitability dynamics does suggest that prior work in vitro [100, 101] and in vivo [6] which has studied these latency dynamics may overestimate the sensi-

tivity of physiological neural excitability to firing rate history.

6.4 Limitations of this study

Dissociated cultures of cortical neurons are known to demonstrate an "extremely rich repertoire" [73] of dynamics at the network level. The range of qualitative dynamics seen in response latency suggest that this also may be true at the level of excitability dynamics of individual neurons. While dissociated cortical cultures lack the same layered structure of cortex in vivo, they do still contain a range of cell types, including pyramidal-shaped excitatory neurons and gabaergic neurons. This cellular diversity of cortex may manifest in studies of activity-dependent excitability as differing degrees of sensitivity to repeated stimulation, as well as qualitative features of response latency, such as jumps in initiation delay following periods of extended response failure. If this variability in latency response originates from cell type, then much larger sample sizes will be necessary for any study of activity-dependent conduction velocity in neurons cultured on high-density MEAs. Progress will therefore be absolutely tied to improvements on experimental yield and reliability of these devices, which at present is highly variable.

Another possibility, however, is that much of the variability seen here may instead be due to small differences in electrode location and stimulation voltage relative to threshold. Indeed, mathematical modeling of the excitability dynamics recorded in cultured neurons responding to repeated stimulation has suggested that stimulation amplitude may be as important as stimulation frequency for determining qualitative features of response to stimulation [102], and measurements of initiation delay [67] have been historically described in the context of stimulation voltage relative to the 50% reliability point [96].

CHAPTER 7
CONCLUSIONS AND FUTURE WORK

7.1 Conclusions

7.1.1 Activity-dependent stimulation reliability varies across stimulation location, though not consistently between the AIS and axon

We find that stimulation reliability at 45 Hz decreases at both the axon and the AIS, relative to stimulation at 1 Hz using the minimum reliable stimulation voltage as found at 1 Hz. This reliability change is not consistent across stimulation locations or across individual cells, though for both stimulation locations the number of evoked APs was well correlated with decreases in the extracellular AP amplitude. This has a major implication regarding the study of activity-dependent excitability, in that studying the activity-dependent effects of stimulation at different parts of the cell requires first answering how this activity can be reliable induced at these different stimulation locations.

We were surprised to find that stimulation at the AIS was not consistently more reliable during 45 Hz stimulation than that at the axon, given the lower stimulation thresholds at the AIS. However, in previous work on high density MEAs[46] did observe a sharp spatial sensitivity of stimulation threshold near the AIS, and found in some instances that stimulation threshold was actually quite high immediately near the location with the minimum threshold. This suggests that the fine features of the regions immediately around the AIS may play important roles in determining it's excitability, which supports the view we argue that intermittent response to stimulation is governed by local excitability dynamics.

7.1.2 Initiation delay is activity-dependent

When stimulation frequency was increased to 45 Hz, initiation delay surpassed propagation delay for both axonal stimulation and AIS stim. We found that the mean latency measured during stimulation at 45 Hz increased relative to 1 Hz for all measured initiation and propagation delays. Further, we found a greater increase in mean initiation delay relative to propagation delay.

This initiation delay suggests that measurements of activity-dependent conduction velocity in the presence of intermittent response are confounded by the contribution of initiation delay. It is unclear at this time, however, at what stimulation frequencies and voltages initiation delay becomes a significant contributor to measured response latency. Prior work on high density MEAs suggests that increasing stimulation may to dampen out some of the variance contributed by initiation delay [67]. However, their work also showed that initiation delay jitter became appreciable before at reliable stimulation voltages. Taking our results and their's together, this suggests that while intermittent response necessary includes variation from initiation delay, latency of response to reliable stimulation may also include substantial initiation delay.

7.2 Future work

Experimentally, further studies of initiation delay should strive to record both antidromic and orthodromic propagation emanating from the site of stimulation. This will assist in distinguishing between initiation delay and propagation delay, with associated clarification of the mechanisms which may be at play in activity-dependent stimulation reliability. Note that this does restrict these measurements to long, straight stretches of axon where response can be recorded on either side of the stimulation site without being distorted by stimulation artifact, a difficult task. It is also suggested that such experiments on activity dependent stimulation reliability move away from the 45 Hz used here and towards clinically relevant

ranges of high frequency stimulation, especially 130 Hz. This choice in stimulation frequency was an artifact of the original aims of this research project, which were motivated by the study of neural computation rather than stimulation reliability.

The local excitability changes governing response to stimulation which we observed in this study suggest that the scale we took to examine the 'location dependence' problem was actually far to wide. Rather than examining stimulation excitability across cellular compartments as disparate as the distal axon and the AIS/soma complex, what is now called for are studies examining the excitability of the axon as stimulation location is varied by the finest degree of control available. The 17 microns between each electrode on high density MEAs is an excellent starting point for this. Tight control of stimulation voltage, set relative to the 50% reliability amplitude and normalized by the relative spread [96] should be required for these experiments, so as to exclude the possibility of reporting artificially high or low reliability due to over or underestimates of the true stimulation threshold, or artificially high estimates of response variability over location due to imprecise calibration of stimulation voltage. While stimulation of axons on high-density MEAs has so far relied on the use of low stimulation voltages to prevent off-target activation [46, 67], the techniques described in this thesis can be used to perform these same experiments with off-target activation. This opens up the range of stimulation voltages, and therefore stimulation locations, where these excitability dynamics can be measured. Varying stimulation electrode location will help to control for variation in the local electrical environment surrounding the point of stimulation, which may be impacted by glia [56, 60].

Future studies on propagation direction should take note of the discrepancies we encountered in stimulation reliability at different locations. Greater control of stimulation reliability than seen in the experiments presented here will be necessary to study the impact of propagation direction on activity-dependent processes. The simplest approach there is to keep stimulation frequency within the ranges where stimulation stays reliable. For neurons grown in the cultures studied here, this is generally 5 Hz and below, though in some cases

neurons have been found which are able to follow rates as high as 20 Hz for minutes at a time.

The idea that extracellular action potential waveform may act as an indicator of 'instantaneous' conduction velocity at a single electrode cluster during activity-dependent slowing warrants further investigation. A simple method of investigating this would be to repeat the same matched filter approach used here, but including multiple waveforms dilated by different levels for each eAP. More advanced methods, such as beamforming or wavelet based approaches, may also be useful. Importantly, if changes in eAP waveform are due primarily to conduction velocity, this implies that the same signal energy is present in the recording, no matter what level of slowing. This means that methods matched to this aspect of the data may not suffer the same loss of accuracy that current approaches do when waveforms adapt over time, potentially improving our ability to measure propagation from highly slowed systems. This would have substantial biological implications, as the lack of clarity when measuring highly slowed systems has so far prevented convincing evidence of branch point failures in these neurons.

The low signal strength of axonal action potentials means that data must be combined from many different recordings to create accurate estimates of their behavior. This was explicit in the analysis of spike triggered and stimulus-triggered averages, where several recordings were averaged together to create a more meaningful description of the neurons under study. However, the same basic principle can be seen at work in the latency estimator, which combines data from multiple electrode clusters before arriving at an estimate of action potential latencies. This is an improvement over traditional spike detection, which estimates spike times based on a relatively limited amount of data, providing further analysis with effectively the wrong input (in this case, spike detections rather than latency estimates). This then requires much data to be discarded, possibly biasing any further estimates.

However, the latency estimator does not complete the inference process either. Latency

estimates were often found to be ridden with outliers, and ad hoc methods needed to be used to continue analysis. Further improvements in the accuracy of these estimates and range of phenomena which can be studied may be made by filling in the gaps between latency estimation and analysis of propagation and initiation delays. Kalman filtering, especially, provides an excellent framework for interpreting latency estimates at multiple points along a propagation path with regards to identifying points at which that estimate is invalid. The assumptions made in Kalman filters, ie that the best a priori estimate of a state variable is whatever it's last observed value was, fit nicely with the relatively slow drift in conduction delay induced by activity-dependent slowing, though may cause issues if used in the context of activity-dependent failures of response to stimulation.

REFERENCES

[1] F. Rattay, "Analysis of models for external stimulation of axons," *IEEE Transactions on Biomedical Engineering*, vol. BME-33, no. 10, pp. 974–977, 1986.

[2] D. A. Wagenaar, J. Pine, and S. M. Potter, "Effective parameters for stimulation of dissociated cultures using multi-electrode arrays," *Journal of Neuroscience Methods*, vol. 138, no. 1-2, pp. 27–37, 2004.

[3] D. Bucher and J.-M. Goaillard, "Beyond faithful conduction: Short-term dynamics, neuromodulation, and long-term regulation of spike propagation in the axon," *Progress in Neurobiology*, vol. 94, no. 4, pp. 307–346, 2011.

[4] K. L. Clark, K. M. Armstrong, and T. Moore, "Probing neural circuitry and function with electrical microstimulation," *Proceedings of the Royal Society of London B: Biological Sciences*, 2011. eprint: `http://rspb.royalsocietypublishing.org/content/early/2011/01/18/rspb.2010.2211.full.pdf`.

[5] A. Veerakumar and O. Berton, "Cellular mechanisms of deep brain stimulation: Activity-dependent focal circuit reprogramming?" *Current Opinion in Behavioral Sciences*, vol. 4, pp. 48–55, 2015.

[6] R. Vardi, A. Goldental, H. Marmari, H. Brama, E. A. Stern, S. Sardi, P. Sabo, and I. Kanter, "Neuronal response impedance mechanism implementing cooperative networks with low firing rates and microsecond precision," *Frontiers in Neural Circuits*, vol. 9, p. 29, 2015.

[7] A. Gal, D. Eytan, A. Wallach, M. Sandler, J. Schiller, and S. Marom, "Dynamics of excitability over extended timescales in cultured cortical neurons," *Journal of Neuroscience*, vol. 30, no. 48, pp. 16 332–16 342, 2010.

[8] H. Marmari, R. Vardi, and I. Kanter, "Chaotic and non-chaotic phases in experimental responses of a single neuron," *Europhysics Letters*, vol. 106, no. 4, p. 46 002, 2014.

[9] C. C. McIntyre and W. M. Grill, "Excitation of central nervous system neurons by nonuniform electric fields," *Biophysical Journal*, vol. 76, no. 2, pp. 878–888, 1999.

[10] ——, "Selective microstimulation of central nervous system neurons," *Annals of Biomedical Engineering*, vol. 28, no. 3, pp. 219–233, 2000.

[11] R. W. Anderson, A. Farokhniaee, K. Gunalan, B. Howell, and C. C. McIntyre, "Action potential initiation, propagation, and cortical invasion in the hyperdirect pathway during subthalamic deep brain stimulation," *Brain Stimulation*, vol. 11, no. 5, pp. 1140–1150, 2018.

[12] N. Poolos, M. Mauk, and J. Kocsis, "Activity-evoked increases in extracellular potassium modulate presynaptic excitability in the ca1 region of the hippocampus," *Journal of Neurophysiology*, vol. 58, no. 2, pp. 404–416, 1987.

[13] F. Zheng, K. Lammert, B. E. Nixdorf-Bergweiler, F. Steigerwald, J. Volkmann, and C. Alzheimer, "Axonal failure during high frequency stimulation of rat subthalamic nucleus," *The Journal of Physiology*, vol. 589, no. 11, pp. 2781–2793, 2011.

[14] Z. Feng, Y. Yu, Z. Guo, J. Cao, and D. M. Durand, "High frequency stimulation extends the refractory period and generates axonal block in the rat hippocampus," *Brain Stimulation*, vol. 7, no. 5, pp. 680–689, 2014.

[15] T. M. Herrington, J. J. Cheng, and E. N. Eskandar, "Mechanisms of deep brain stimulation," *Journal of Neurophysiology*, vol. 115, no. 1, pp. 19–38, 2015.

[16] C. C. McIntyre and R. W. Anderson, "Deep brain stimulation mechanisms: The control of network activity via neurochemistry modulation," *Journal of Neurochemistry*, vol. 139, pp. 338–345, 2016.

[17] L. Nowak and J Bullier, "Axons, but not cell bodies, are activated by electrical stimulation in cortical gray matter i. evidence from chronaxie measurements," *Experimental Brain Research*, vol. 118, no. 4, pp. 477–488, 1998.

[18] W. M. Grill, A. N. Snyder, and S. Miocinovic, "Deep brain stimulation creates an informational lesion of the stimulated nucleus," *Neuroreport*, vol. 15, no. 7, pp. 1137–1140, 2004.

[19] R. Rosenbaum, A. Zimnik, F. Zheng, R. S. Turner, C. Alzheimer, B. Doiron, and J. E. Rubin, "Axonal and synaptic failure suppress the transfer of firing rate oscillations, synchrony and information during high frequency deep brain stimulation," *Neurobiology of Disease*, vol. 62, pp. 86–99, 2014.

[20] Q. Li, Y. Ke, D. C. Chan, Z.-M. Qian, K. K. Yung, H. Ko, G. W. Arbuthnott, and W.-H. Yung, "Therapeutic deep brain stimulation in parkinsonian rats directly influences motor cortex," *Neuron*, vol. 76, no. 5, pp. 1030–1041, 2012.

[21] W. M. Grill, M. B. Cantrell, and M. S. Robertson, "Antidromic propagation of action potentials in branched axons: Implications for the mechanisms of action of deep brain stimulation," *Journal of Computational Neuroscience*, vol. 24, no. 1, pp. 81–93, 2008.

[22] D. Debanne, E. Campanac, A. Bialowas, E. Carlier, and G. Alcaraz, "Axon physiology," *Physiological Reviews*, vol. 91, no. 2, pp. 555–602, 2011.

[23] Y Grossman, I Parnas, and M. Spira, "Differential conduction block in branches of a bifurcating axon.," *The Journal of Physiology*, vol. 295, no. 1, pp. 283–305, 1979.

[24] J. P. Meeks and S. Mennerick, "Selective effects of potassium elevations on glutamate signaling and action potential conduction in hippocampus," *Journal of Neuroscience*, vol. 24, no. 1, pp. 197–206, 2004.

[25] A. Soleng, K Chiu, and M Raastad, "Unmyelinated axons in the rat hippocampus hyperpolarize and activate an h current when spike frequency exceeds 1 hz," *The Journal of Physiology*, vol. 552, no. 2, pp. 459–470, 2003.

[26] A. W. Ballo, F. Nadim, and D. Bucher, "Dopamine modulation of ih improves temporal fidelity of spike propagation in an unmyelinated axon," *Journal of Neuroscience*, vol. 32, no. 15, pp. 5106–5119, 2012.

[27] T. H. Bullock, "Facilitation of conduction rate in nerve fibres," *The Journal of Physiology*, vol. 114, no. 1-2, pp. 89–97, 1951.

[28] H. A. Swadlow, "Systematic variations in the conduction velocity of slowly conducting axons in the rabbit corpus callosum," *Experimental Neurology*, vol. 43, no. 2, pp. 445–451, 1974.

[29] R. Miller and J Rinzel, "The dependence of impulse propagation speed on firing frequency, dispersion, for the hodgkin-huxley model," *Biophysical Journal*, vol. 34, no. 2, pp. 227–259, 1981.

[30] C. Weidner, M. Schmelz, R. Schmidt, B. Hammarberg, K. Ørstavik, M. Hilliges, H. E. Torebjörk, and H. O. Handwerker, "Neural signal processing: The underestimated contribution of peripheral human c-fibers," *Journal of Neuroscience*, vol. 22, no. 15, pp. 6704–6712, 2002.

[31] J. Thalhammer, S. Raymond, F. Popitz-Bergez, and G. Strichartz, "Modality-dependent modulation of conduction by impulse activity in functionally characterized single cutaneous afferents in the rat," *Somatosensory & Motor Research*, vol. 11, no. 3, pp. 243–257, 1994.

[32] J. Tigerholm, M. E. Petersson, O. Obreja, A. Lampert, R. Carr, M. Schmelz, and E. Fransén, "Modeling activity-dependent changes of axonal spike conduction in primary afferent c-nociceptors," *Journal of Neurophysiology*, vol. 111, no. 9, pp. 1721–1735, 2013.

[33] A. L. Hodgkin and A. F. Huxley, "A quantitative description of membrane current and its application to conduction and excitation in nerve," *The Journal of Physiology*, vol. 117, no. 4, pp. 500–544, 1952.

[34] S. Raymond, "Effects of nerve impulses on threshold of frog sciatic nerve fibres.," *The Journal of Physiology*, vol. 290, no. 2, pp. 273–303, 1979.

[35] J. Kocsis and C. VanderMaelen, "A supernormal period in central axons following single cell stimulation," *Experimental Brain Research*, vol. 36, no. 2, pp. 381–386, 1979.

[36] H. Swadlow, D. Rosene, and S. Waxman, "Characteristics of interhemispheric impulse conduction between prelunate gyri of the rhesus monkey," *Experimental Brain Research*, vol. 33, no. 3-4, pp. 455–467, 1978.

[37] H. Swadlow and S. Waxman, "Observations on impulse conduction along central axons," *Proceedings of the National Academy of Sciences*, vol. 72, no. 12, pp. 5156–5159, 1975.

[38] R. De Col, K. Messlinger, and R. W. Carr, "Repetitive activity slows axonal conduction velocity and concomitantly increases mechanical activation threshold in single axons of the rat cranial dura," *The Journal of Physiology*, vol. 590, no. 4, pp. 725–736, 2012.

[39] A. Gardner-Medwin, "An extreme supernormal period in cerebellar parallel fibres," *The Journal of Physiology*, vol. 222, no. 2, pp. 357–371, 1972.

[40] R FitzHugh and H. Antosiewicz, "Automatic computation of nerve excitationdetailed corrections and additions," *Journal of the Society for Industrial and Applied Mathematics*, vol. 7, no. 4, pp. 447–458, 1959.

[41] J. R. Clay, "A stochastic analysis of the graded excitatory response of nerve membrane," *Journal of Theoretical Biology*, vol. 59, no. 1, pp. 141–158, 1976.

[42] J. R. Clay and L. J. DeFelice, "Relationship between membrane excitability and single channel open-close kinetics," *Biophysical journal*, vol. 42, no. 2, pp. 151–157, 1983.

[43] M. K. Lewandowska, M. Radivojević, D. Jäckel, J. Müller, and A. R. Hierlemann, "Cortical axons, isolated in channels, display activity-dependent signal modulation as a result of targeted stimulation," *Frontiers in Neuroscience*, vol. 10, p. 83, 2016.

[44] H. E. Torebjörk and R. G. Hallin, "Responses in human a and c fibres to repeated electrical intradermal stimulation," *Journal of Neurology, Neurosurgery & Psychiatry*, vol. 37, no. 6, pp. 653–664, 1974.

[45] R. Habibey, S. Latifi, H. Mousavi, M. Pesce, E. Arab-Tehrany, and A. Blau, "A multielectrode array microchannel platform reveals both transient and slow changes in axonal conduction velocity," *Scientific Reports*, vol. 7, no. 1, p. 8558, 2017.

[46] M. Radivojevic, D. Jäckel, M. Altermatt, J. Müller, V. Viswam, A. Hierlemann, and D. J. Bakkum, "Electrical identification and selective microstimulation of neuronal compartments based on features of extracellular action potentials," *Scientific Reports*, vol. 6, p. 31 332, 2016.

[47] M. Popovic, K. Vogt, K. Holthoff, A. Konnerth, B. M. Salzberg, A. Grinvald, S. D. Antic, M. Canepari, and D. Zecevic, "Imaging submillisecond membrane potential changes from individual regions of single axons, dendrites and spines," in *Membrane Potential Imaging in the Nervous System and Heart*, Springer, 2015, pp. 57–101.

[48] N. Jaafari, K. E. Vogt, P. Saggau, L. M. Leslie, D. Zecevic, and M. Canepari, "Combining membrane potential imaging with other optical techniques," in *Membrane Potential Imaging in the Nervous System and Heart*, Springer, 2015, pp. 103–125.

[49] R Stämpfli, "A new method for measuring membrane potentials with external electrodes," *Experientia*, vol. 10, no. 12, pp. 508–509, 1954.

[50] J. Ritchie and R. Straub, "The hyperpolarization which follows activity in mammalian non-medullated fibres," *The Journal of Physiology*, vol. 136, no. 1, pp. 80–97, 1957.

[51] D. Palani, D. Pekala, A. Baginskas, H. Szkudlarek, and M. Raastad, "Action potentials recorded from bundles of very thin, gray matter axons in rat cerebellar slices using a grease-gap method," *Journal of Neuroscience Methods*, vol. 208, no. 2, pp. 119–127, 2012.

[52] J. M. Barry, "Axonal activity in vivo: Technical considerations and implications for the exploration of neural circuits in freely moving animals," *Frontiers in Neuroscience*, vol. 9, p. 153, 2015.

[53] J. Müller, M. Ballini, P. Livi, Y. Chen, M. Radivojevic, A. Shadmani, V. Viswam, I. L. Jones, M. Fiscella, R. Diggelmann, *et al.*, "High-resolution cmos mea platform to study neurons at subcellular, cellular, and network levels," *Lab on a Chip*, vol. 15, no. 13, pp. 2767–2780, 2015.

[54] M. E. J. Obien, K. Deligkaris, T. Bullmann, D. J. Bakkum, and U. Frey, "Revealing neuronal function through microelectrode array recordings," *Frontiers in Neuroscience*, vol. 8, p. 423, 2015.

[55] G. Zeck, A. Lambacher, and P. Fromherz, "Axonal transmission in the retina introduces a small dispersion of relative timing in the ganglion cell population response," *PLoS One*, vol. 6, no. 6, e20810, 2011.

[56] D. J. Bakkum, U. Frey, M. Radivojevic, T. L. Russell, J. Müller, M. Fiscella, H. Takahashi, and A. Hierlemann, "Tracking axonal action potential propagation on a high-density microelectrode array across hundreds of sites," *Nature Communications*, vol. 4, p. 2181, 2013.

[57] K. Deligkaris, T. Bullmann, and U. Frey, "Extracellularly recorded somatic and neuritic signal shapes and classification algorithms for high-density microelectrode array electrophysiology," *Frontiers in Neuroscience*, vol. 10, p. 421, 2016.

[58] M. K. Lewandowska, D. J. Bakkum, S. B. Rompani, and A. Hierlemann, "Recording large extracellular spikes in microchannels along many axonal sites from individual neurons," *PloS One*, vol. 10, no. 3, e0118514, 2015.

[59] D. J. Bakkum, M. Radivojevic, M. E. Obien, D. Jaeckel, U. Frey, H. Takahashi, and A. Hierlemann, "The axon initial segment drives the neuron's extracellular action potential," *BioRxiv*, p. 266 734, 2018.

[60] K. R. Tovar, D. C. Bridges, B. Wu, C. Randall, M. Audouard, J. Jang, P. K. Hansma, and K. S. Kosik, "Action potential propagation recorded from single axonal arbors using multi-electrode arrays," *Journal of Neurophysiology*, 2018.

[61] U. Frey, J. Sedivy, F. Heer, R. Pedron, M. Ballini, J. Mueller, D. Bakkum, S. Hafizovic, F. D. Faraci, F. Greve, *et al.*, "Switch-matrix-based high-density microelectrode array in cmos technology," *IEEE Journal of Solid-State Circuits*, vol. 45, no. 2, pp. 467–482, 2010.

[62] U Frey, U Egert, F Heer, S Hafizovic, and A. Hierlemann, "Microelectronic system for high-resolution mapping of extracellular electric fields applied to brain slices," *Biosensors and Bioelectronics*, vol. 24, no. 7, pp. 2191–2198, 2009.

[63] C. Gold, D. A. Henze, C. Koch, and G. Buzsaki, "On the origin of the extracellular action potential waveform: A modeling study," *Journal of Neurophysiology*, vol. 95, no. 5, pp. 3113–3128, 2006.

[64] J Lipski, "Antidromic activation of neurones as an analytic tool in the study of the central nervous system," *Journal of Neuroscience Methods*, vol. 4, no. 1, pp. 1–32, 1981.

[65] H. A. Swadlow, "Antidromic activation: Measuring the refractory period at the site of axonal stimulation," *Experimental Neurology*, vol. 75, no. 2, pp. 514–519, 1982.

[66] C. R. Stoelzel, Y. Bereshpolova, J.-M. Alonso, and H. A. Swadlow, "Axonal conduction delays, brain state, and corticogeniculate communication," *Journal of Neuroscience*, pp. 0444–17, 2017.

[67] M. Radivojevic, F. Franke, M. Altermatt, J. Müller, A. Hierlemann, and D. J. Bakkum, "Tracking individual action potentials throughout mammalian axonal arbors," *ELife*, vol. 6, 2017.

[68] Z. Feng, Z. Wang, Z. Guo, W. Zhou, Z. Cai, and D. M. Durand, "High frequency stimulation of afferent fibers generates asynchronous firing in the downstream neurons in hippocampus through partial block of axonal conduction," *Brain Research*, vol. 1661, pp. 67–78, 2017.

[69] F. Franke, R. Q. Quiroga, A. Hierlemann, and K. Obermayer, "Bayes optimal template matching for spike sorting–combining fisher discriminant analysis with optimal filtering," *Journal of Computational Neuroscience*, vol. 38, no. 3, pp. 439–459, 2015.

[70] C. M. Hales, J. D. Rolston, and S. M. Potter, "How to culture, record and stimulate neuronal networks on micro-electrode arrays (meas)," *Journal of Visualized Experiments: JoVE*, no. 39, 2010.

[71] Y Jimbo, T Tateno, and H. Robinson, "Simultaneous induction of pathway-specific potentiation and depression in networks of cortical neurons," *Biophysical Journal*, vol. 76, no. 2, pp. 670–678, 1999.

[72] R Matsumura, H Yamamoto, M Niwano, and A Hirano-Iwata, "An electrically resistive sheet of glial cells for amplifying signals of neuronal extracellular recordings," *Applied Physics Letters*, vol. 108, no. 2, p. 023 701, 2016.

[73] D. A. Wagenaar, J. Pine, and S. M. Potter, "An extremely rich repertoire of bursting patterns during the development of cortical cultures," *BMC Neuroscience*, vol. 7, no. 1, p. 11, 2006.

[74] D. Wagenaar, T. B. DeMarse, and S. M. Potter, "Meabench: A toolset for multi-electrode data acquisition and on-line analysis," in *Neural Engineering, 2005. Conference Proceedings. 2nd International IEEE EMBS Conference on*, IEEE, 2005, pp. 518–521.

[75] MathWorks, *Matlab*, version 2012.

[76] D. A. Wagenaar and S. M. Potter, "Real-time multi-channel stimulus artifact suppression by local curve fitting," *Journal of Neuroscience Methods*, vol. 120, no. 2, pp. 113–120, 2002.

[77] M. S. Fee, P. P. Mitra, and D. Kleinfeld, "Automatic sorting of multiple unit neuronal signals in the presence of anisotropic and non-gaussian variability," *Journal of Neuroscience Methods*, vol. 69, no. 2, pp. 175–188, 1996.

[78] D. N. Hill, S. B. Mehta, and D. Kleinfeld, "Quality metrics to accompany spike sorting of extracellular signals," *Journal of Neuroscience*, vol. 31, no. 24, pp. 8699–8705, 2011.

[79] D. J. Bakkum, Z. C. Chao, and S. M. Potter, "Long-term activity-dependent plasticity of action potential propagation delay and amplitude in cortical networks," *PLOS One*, vol. 3, no. 5, e2088, 2008.

[80] C. M. Hales, R. Zeller-Townson, J. P. Newman, J. T. Shoemaker, N. J. Killian, and S. M. Potter, "Stimulus-evoked high frequency oscillations are present in neuronal networks on microelectrode arrays," *Frontiers in Neural Circuits*, vol. 6, p. 29, 2012.

[81] P. Boeijinga and F. L. da Silva, "A new method to estimate time delays between eeg signals applied to beta activity of the olfactory cortical areas," *Electroencephalography and Clinical Neurophysiology*, vol. 73, no. 3, pp. 198–205, 1989.

[82] J. P. Pijn and F. L. da Silva, "Propagation of electrical activity: Nonlinear associations and time delays between eeg signals," in *Basic Mechanisms of the EEG*, Springer, 1993, pp. 41–61.

[83] N. Mars, "Time delay estimator for eeg analysis based on information theory," in *Acoustics, Speech, and Signal Processing, IEEE International Conference on ICASSP'82.*, IEEE, vol. 7, 1982, pp. 733–735.

[84] M. Zivanovic, "Time-varying multicomponent signal modeling for analysis of surface emg data," *IEEE Signal Processing Letters*, vol. 21, no. 6, pp. 692–696, 2014.

[85] C. FU, S.-l. LIAN, and Q. LI, "The re-sampling technique application in action potential conduction velocity estimation of surface electromyography," *Progress in Modern Biomedicine*, vol. 19, p. 056, 2011.

[86] P. Ravier, D. Farina, and O. Buttelli, "Time-varying delay estimators for measuring muscle fiber conduction velocity from the surface electromyogram," *Biomedical Signal Processing and Control*, vol. 22, pp. 126–134, 2015.

[87] G.-T. Luu, T. D. Tran, H. Tan, T. T. Ngo, P. Ravier, and O. Buttelli, "Time varying delay estimators for measuring muscle fiber conduction veloity: Effects of non-stationarity of the data," in *International Conference on the Development of Biomedical Engineering in Vietnam*, Springer, 2017, pp. 415–419.

[88] P. Laguna, R. Jané, and P. Caminal, "A time delay estimator based on the signal integral: Theoretical performance and testing on ecg signals," *IEEE Transactions on Signal Processing*, vol. 42, no. 11, pp. 3224–3229, 1994.

[89] G. Van der Vliet, J Holsheimer, and D Bingmann, "Calculation of the conduction velocity of short nerve fibres," *Medical and Biological Engineering and Computing*, vol. 18, no. 6, pp. 749–757, 1980.

[90] V. S. Jasrotia and P. A. Parker, "Matched filters in nerve conduction velocity estimation," *IEEE Transactions on Biomedical Engineering*, no. 1, pp. 1–9, 1983.

[91] G. McVicar and P. Parker, "Spectrum dip estimator of nerve conduction velocity," *IEEE Transactions on Biomedical Engineering*, vol. 35, no. 12, pp. 1069–1076, 1988.

[92] A. A. Faisal and S. B. Laughlin, "Stochastic simulations on the reliability of action potential propagation in thin axons," *PLoS Computational Biology*, vol. 3, no. 5, e79, 2007.

[93] C. C. McIntyre and W. M. Grill, "Extracellular stimulation of central neurons: Influence of stimulus waveform and frequency on neuronal output," *Journal of Neurophysiology*, vol. 88, no. 4, pp. 1592–1604, 2002.

[94] M. H. Kole and G. Stuart, "Is action potential threshold lowest in the axon," *Nature Neuroscience*, vol. 11, pp. 1253–1255, 2008.

[95] W. Hu, C. Tian, T. Li, M. Yang, H. Hou, and Y. Shu, "Distinct contributions of na v 1.6 and na v 1.2 in action potential initiation and backpropagation," *Nature Neuroscience*, vol. 12, no. 8, p. 996, 2009.

[96] A. Verveen and H. Derksen, "Fluctuation phenomena in nerve membrane," *Proceedings of the IEEE*, vol. 56, no. 6, pp. 906–916, 1968.

[97] Z. Feng, X. Zheng, Y. Yu, and D. M. Durand, "Functional disconnection of axonal fibers generated by high frequency stimulation in the hippocampal ca1 region invivo," *Brain Research*, vol. 1509, pp. 32–42, 2013.

[98] R. De Col, K. Messlinger, and R. W. Carr, "Conduction velocity is regulated by sodium channel inactivation in unmyelinated axons innervating the rat cranial meninges," *The Journal of Physiology*, vol. 586, no. 4, pp. 1089–1103, 2008.

[99] S. M. Sherman and R. Guillery, "On the actions that one nerve cell can have on another: Distinguishing "drivers" from "modulators"," *Proceedings of the National Academy of Sciences*, vol. 95, no. 12, pp. 7121–7126, 1998.

[100] R. Vardi, R. Timor, S. Marom, M. Abeles, and I. Kanter, "Synchronization by elastic neuronal latencies," *Physical Review E*, vol. 87, no. 1, p. 012 724, 2013.

[101] R. Vardi, H. Marmari, and I. Kanter, "Error correction and fast detectors implemented by ultrafast neuronal plasticity," *Physical Review E*, vol. 89, no. 4, p. 042 712, 2014.

[102] D. Soudry and R. Meir, "Conductance-based neuron models and the slow dynamics of excitability," *Frontiers in Computational Neuroscience*, vol. 6, p. 4, 2012.